IMPURITY PROFILING AND DEGRADATION STUDY OF CICLOPIROX OLAMINE

5.1 SELECTION OF DRUG

HOE 296 was the original name of an off patent drug ciclopirox olamine (CIO) when it was first reported as a potential antifungal agent in 1973 (1). CIO is a hydroxypyridone derivative which differs in structure and antifungal activity from other known antifungal agents. It was discovered as broad spectrum antifungal agent that inhibits nearly all yeasts and moulds, dermatodhytes and also includes *candida* species resistant to azoles like *candida krusei*, *candida guilliermondii* and *candida glabrata*. CIO also has proven antibacterial activity against pathogenic gram positive and gram negative bacteria's (2).

CIO has been clinically used for treatment of mycoses of the nails and skin for over two decades and most of the studies dealing with the mode of action of this drug were published approximately 20 years ago, at the time when CIO was synthesized and introduced into clinical therapy (2-6). When the usage of drug became more frequent, the results of many investigations about its efficacy were reported and comparisons of its clinical effectiveness with other available antimicrobial agents were published. The new potential application of CIO involves the treatment of solid tumors hence CIO could be repurposed for its new indication as an anticancer agent based on prior safety and toxicity testing in animals and humans (7).

Despite of tremendous use of CIO as an antifungal agent and its new indications, literature review revealed that there have been no reports on impurity profiling, stress degradation and structural characterization of the degradation related impurities of CIO, up to our knowledge. Hence, the investigation was undertaken to study the impurity profile and degradation study of the drug CIO under different stress conditions. The structure of degradation products were proposed by LC-MS/MS study and fragmentation pathways were outlined.

5.2 DRUG PROFILE

General Properties

IUPAC Name: 6-Cyclohexyl-1-hydroxy-4-methyl-1,2-dihydropyridin-2-one and 2-aminoethanol.

Molecular Formula: $C_{14}H_{24}N_2O_3$

Molecular Weight: 268.4

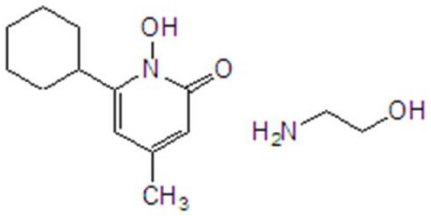

Figure 5.1 : Chemical Structure of Ciclopirox Olamine

Chemical Structure:

Physiochemical Properties (8)

Appearance: white or pale yellow crystalline or amorphous powder.

Melting point: 143 °C

logP: 2.3

pKa: (strongest acidic)- 6.84, *(strongest basic)*-6.2

Solubility: Partially soluble in water; soluble in methanol, ethanol, and acetonitrile; slightly soluble in ethyl acetate; insoluble in cyclohexane

Drug Category: Antifungal agent

Mechanism of action (9-11): Unlike known antifungals such as terbinafine and itraconazole that affect sterol synthesis, ciclopirox act through the chelation of polyvalent metal cations like Al^{3+} and Fe^{3+}. These cations disrupt cellular activities such as mitochondrial electron transport processes and energy production by inhibiting many enzymes including cytochromes. Ciclopirox causes disorganization of internal structures and also modify the plasma membrane of fungi. The inhibition of cyclooxygenase and 5-lipoxygenase leads to antiinflammatory effect of ciclopirox. The ciclopirox may exert its

effect by disrupting cell division signals, DNA repair and structures of mitotic spindles, as well as some elements of intracellular transport system.

Uses: Used for topical treatment of mild to moderate onychomycosis of fingernails and toenails due to *Trichophyton rubrum,* in immune-competent patients.

Marketed Formulation: Cream (Batrafan by Sanofi Aventis),

Lotion (Stieprox by Stiefel India Pvt Ltd), and

Solution (Onylac by Cipla Limited)

5.3 LITERATURE REVIEW

Literature review reveals that different analytical methods were reported for the estimation of CIO based on diverse analytical instrumentation and methodologies. These includes spectrophotometric (12), chromatographic (13-18) , microbiological (19) capillary electrophoresis (20) and polarographic methods (21, 22). There is a report on stability indicating RP-HPLC assay method (23) of CIO but identification and characterization of degradation products were not done. Also precolumn derivatization of CIO was not carried out wherein literature clearly indicates that direct quantification of CIO by either reverse phase or normal phase chromatography is difficult. The N-hydroxyl pyridone group present in CIO showed strong interaction with trace metal ions in assay and solvent systems, and also with silica gel based HPLC adsorbents through a chelating effect. This results in severe peak tailing and non-linearity of responses i.e. peak area versus concentration of CIO. A modification of the stationary phase for RP-HPLC method was reported for the estimation of ciclopirox in antidandruff formulations that involves several steps for chemical modification and deactivation of the silanol groups and heavy metal cation contents to reduce the chelating complexation (24). The HPLC method described in USP requires extended time washing for at least 15 h and equilibration for 5 h before a new method could be used in the experiment to ensure the desorption and complete removal of disruptive metal ions. However, it still gives a badly tailed peak and leads to poor quantitation (25).

Few literature cite the pre-column derivatization methods, (26) to eliminate the chelating effect by methylation of the N-hydroxyl group to enable the quantification of CIO. Two

different methods were described for methylation of N-hydroxyl group of CIO in literature, these are:

a) Derivatization, of N-hydroxyl group by methyl iodide in basic condition by 1 M sodium hydroxide. The reaction was carried out in ice bath. The excess of methyl iodide was removed by adding 25% ammonium hydroxide solution to the mixture (14).

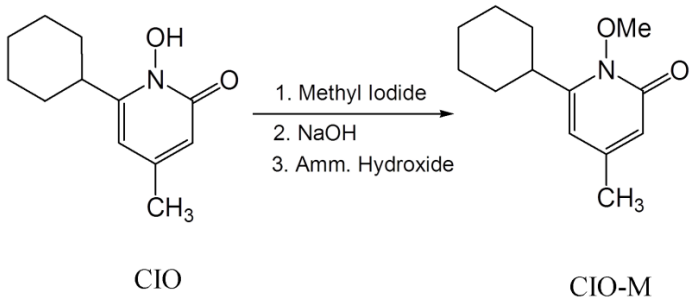

CIO CIO-M

Figure 5.2 : Methylation of Ciclopirox Olamine by methyl iodide

b) Derivatization, of N-hydroxyl group by dimethyl sulfate in basic condition by 2 M sodium hydroxide. The reaction was carried out at room temperature. The excess of dimethyl sulfate was removed by adding equivalent amount of triethyl amine (15).

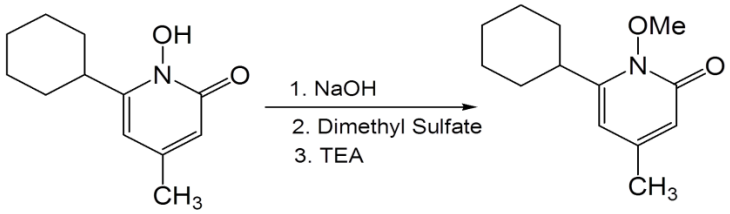

CIO CIO-M

Figure 5.3: Methylation of Ciclopirox Olamine by dimethyl sulfate

5.4. SECTION –A

DEVELOPMENT AND VALIDATION OF QbD BASED STABILITY INDICATING RP-HPLC METHOD

5.4.1 EXPERIMENTAL

5.4.1.1 Chemicals and Reagents

CIO bulk drug was obtained as gift samples from Glenmark Pharmaceuticals limited, Mumbai. Other chemicals and regents were same as described in section 3.4.1.1.

5.4.1.2 Equipments and Chromatographic Conditions

The equipments utilized in present experiment were same as in section 3.4.1.2. Separation was accomplished on a Phenomenex RP- C18 column (250 ×4.6 mm, 5 µm) at wavelength of 300 nm. The mobile phase consisted of a mixture of 20 mM ammonium acetate buffer (pH adjusted to 5.7 with glacial acetic acid) and MeOH/ACN (90:10) in the ratio 66:44, v/v at a flow-rate of 1.1 ml/min with isocratic elution. The mobile phase was filtered using 0.2 µm disposable filters (Ultipore, PALL lifesciences, 40 mm) and degassed by ultra-sonication prior to use. The analysis was performed at ambient temperature with injection volume of 20 µL.

5.4.1.3 Preparation of Stock, Sample and Buffer solutions

Stock solutions were prepared in ACN at a concentration of 1 mg/ml. In the present work derivatization of CIO was carried out by method b) described by Lehr K. H. (15) for direct quantitation of the 1-methoxy derivative of CIO in commercial dosage forms (Lotion). After derivatization, the working standards were prepared in mobile phase to produce 20 – 120 µg/ml of CIO. To analyze the stressed samples suitable dilutions were made after derivatization in mobile phase to obtain the final concentration of 110 µg/ml with respect to CIO. Same aliquots i.e. 20- 120 µg/ml of CIO were prepared for recovery studies and assay of marketed formulation after derivatization.

Acetate buffer (20mM) was prepared by dissolving 0.70 gm of anhydrous ammonium acetate in 500 ml of double distilled water and adjusted to pH 5.7 using glacial acetic acid which was finally filtered with 0.2 mm Nylon membrane filter and degassed by ultrasonication for 5 minutes.

Derivatization: For derivatization, 0.5 ml of 2 M sodium hydroxide solution and 200 µl of dimethyl sulphate were added to the 1 ml of CIO (2 mg/ml), the mixture was vortexed for two min and kept at 37°C for 15-20 min. Subsequently, 200 µl of triethylamine were added and was vortexed again. The solution was diluted to desired strength with mobile phase, and filtered through syringe filter. Placebo samples (without drug) were also prepared.

5.4.1.4 Preparation of Degradation Products (DPs)

For the stress degradation studies, different stress conditions were used for bulk drug. Placebo samples (without drug) were also prepared for comparison with the stress degradation samples. A preliminary study was performed to gain some basic information about the stability of the compound. Then for final study the drug was stressed to maximum condition where 10-80% degradation occurred.

The same stress degradation study was also performed on marketed formulation of CIO (Lotion, Stieprox by Stiefel India Pvt Ltd) to determine formation of any DPs due to drug excipient interaction.

The stress degradation conditions were as follows:

Hydrolytic Degradation (Acid/Base/Neutral Hydrolysis):

1 mg/ml of CIO in freshly prepared 1 N HCl/ 0.5 N NaOH was prepared by sonication for 10 seconds in an ultrasonicator bath. Solutions were refluxed at 80^0C in dark for 12 hrs for acid hydrolysis and 10 hrs for base hydrolysis. Aliquot of 2 mL of these samples were withdrawn neutralized with NaOH/HCl and stored in freezer before analysis. For neutral hydrolysis sample was prepared in double distilled water and refluxed at 100^0C in dark for 12 hrs.

Oxidative (Peroxide- induced) Degradation:

For oxidative degradation study 1 mg/ml of CIO was prepared in 6% H_2O_2. The solution was refluxed at 100^0C in dark for 6 hour.

Photolytic Degradation:

For the photochemical stability, solid drug (API) was spread in 1mm thickness on a petridish and exposed to 5382 LUX and 144UW/cm^2 for 21 days.

Thermal (Dry heat induced) Degradation:

For preparing dry heat degradation product, solid drugs (API) was spread in 1mm thickness on a petridish and placed in oven at 80ºC for 21 days under dry heat condition in the dark.

Thermal-Humidity Induced Degradation:

Solid drug (API) was placed in stability chamber at 40ºC±2º C and 75±5 % RH for 21 days.

All the stress degraded samples were derivatized as described in method b), suitably diluted with mobile phase to make final concentration of 110 ppm and filtered through 0.2µ nylon membrane syringe filter prior to injection in HPLC.

5.4.1.5 Method Development

Analytical target profile (ATP)

The ATP was defined and here in present study the ATP is

1) To develop stability indicating liquid chromatographic method that shows well resolved, sharp and asymmetric peak of CIO.

2) The drug peaks should be separated with peaks of DPs.

3) The resolved peaks should be acquired in shorter run time.

Preliminary investigations

To select the initial HPLC analysis conditions, preliminary investigations were carried out. The analysis was performed with working standard solution of CIO and mixture of DPs (showing 10-80% decrease in peak area of CIO) were prepared by appropriate dilution of the stock solution of drugs and DPs (1 mg/ml) in water and ACN. The analysis was performed using a Phenomenex Luna RP C-18 column due to its high stability in a broad pH range (pH 2-9). The feasibilities of various solvent systems involving ACN, methanol, and buffer in different compositions in isocratic/gradient elution modes and flow rates were measured to acquire a good peak shape and resolution of CIO and DPs. It has been observed that the isocratic elution with ACN provides better separation with good peak shape and shorter run time. The effect of ratio of methanol with ACN was also studied to

obtain resolution among CIO and DPs. Chromatograms of some preliminary trials are shown in figure 5.1.

The preliminary observations revealed that the ratio of ACN during the isocratic elution was critical for good peak shape of CIO and DPs. pH of mobile phase is crucial because some DPs do not elute at particular pH especially DP-1 and DP-2. The UV absorption maximum for CIO is at 300.2 nm, whereas DPs may have different absorption maxima. So, absorbance of DPs were extracted through PDA detector to select appropriate wavelength for estimation of CIO and DPs. The temperature at which analysis was carried out also affects the retention time (Rt), sensitivity and sometimes peak symmetry of some analyte. The flow rate of mobile phase is also a critical parameter in terms of solvent consumption, peak broadening and resolution.

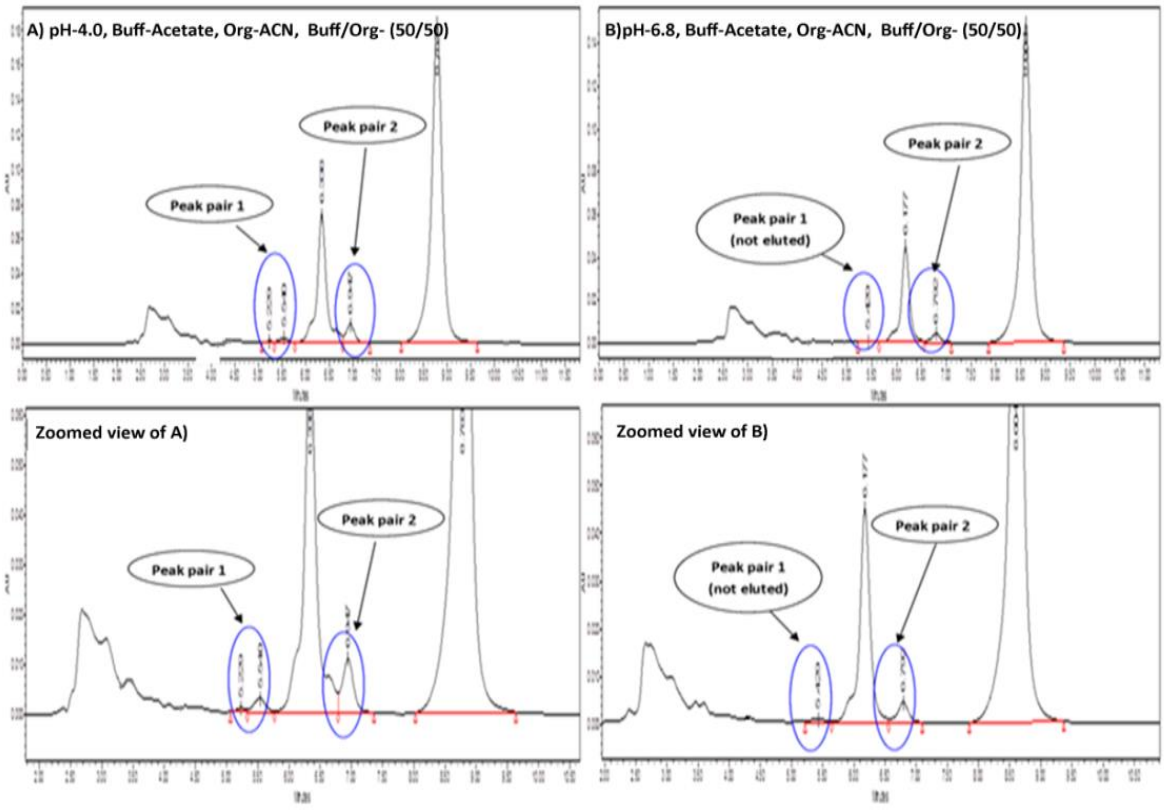

Figure 5.4 : Chromatograms of preliminary trials

Risk assessment by cause- effect relationship and CNX approach

For risk assessment a fishbone diagram (or Ishikawa diagram) was build to identify potential factors and relate them to the requirement specified in the ATP (27). Then a CNX approach was utilized to identify high risk variables affecting the analytical attributes. Three critical method variables viz. percentage of organic in mobile phase, and pH of mobile phase were identified with highest scores. These variables were designated primary factors and subjected to response surface optimization. Other variables with marginal score, designated secondary factors were subjected to PBD screening before response surface optimization to develop a robust and reliable HPLC method.

Design of Experiments

Plackett Burman screening design (PBD): The PBD with 12 runs was initially used to estimate the main effects of six secondary factors selected after CNX risk assessment. To provide a measure of process stability and inherent variability, two center points were also added in the PBD.

Central Composite response surface design (CCD): The CCD with 20 runs including six center points was used. The significant factors selected after CNX risk assessment and PB screening design were subjected to CCD to evaluate the main and interaction effects and to optimize the HPLC analysis conditions.

5.4.1.6 Method validation using ICH Q2(R1) guideline and total error approach

The present method was validated according to the ICH (28) and the ISO-17025 guidelines applying accuracy profiles based on the "total error" approach (29). In the present method response function, precision, accuracy and trueness were determined by total error approach and linearity and range, limit of detection, limit of quantification and robustness were determined as per ICH Q2(R1) guideline.

5.4.1.7 Uncertainty of measurement (UM)

Since few factors were not included in the validation such as errors during mass of sample taken there may be some doubts in the results, although the method was validated. So uncertainty estimation was carried out and compiled up with the Expanded Uncertainty (EU) and Relative Expanded Uncertainty (REU) results.

5.4.1.8 Application of developed HPLC method

The developed SIAM was applied to analysis of CIO in formulation. Stress degradation was carried out in formulation and % degradation was calculated.

5.4.2 RESULTS AND DISCUSSION

5.4.2.1 Determination of suitable wavelength

The UV spectrum of CIO was recorded in the range 200-400 nm is presented in figure 5.5. The spectrum indicated that the λ_{max} of CIO is 300 nm.

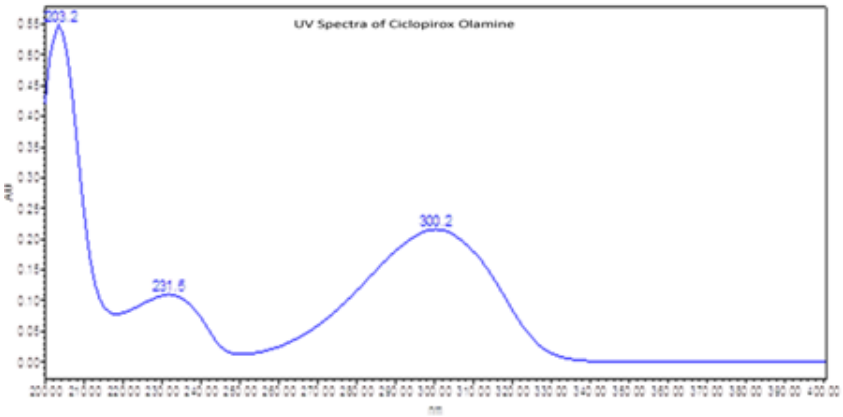

Figure 5.5: UV Spectra of CIO

The UV spectra of CIO and its DPs were extracted in PDA detector from 200-400 nm and are shown in figure 5.6. The spectrum indicated that 300 nm gives a good absorption and sensitivity for DPs and CIO.

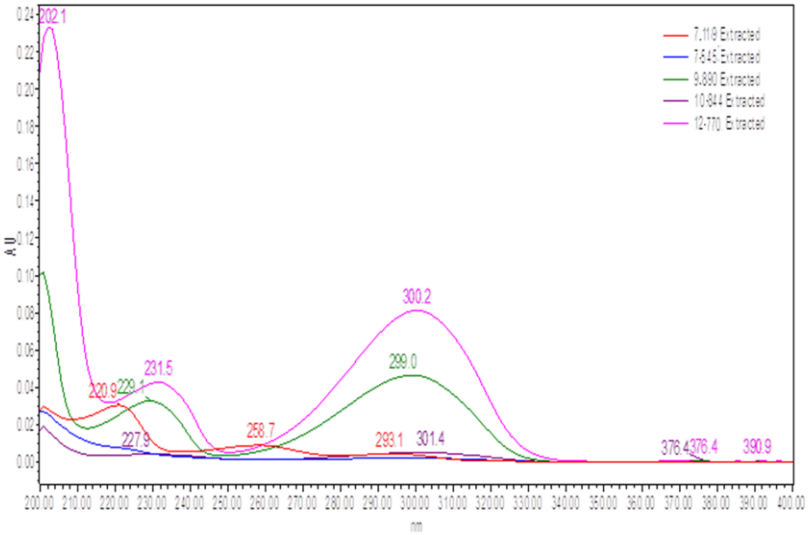

Figure 5.6: UV spectra of CIO and DPs extracted from PDA

5.4.2.2 Method optimization and development

5.4.2.2.1 ATP

Based on preliminary investigation, the parameters that will be focused in our method development were selected and enlisted as ATP.

5.4.2.2.2 Risk assessment by cause- effect relationship and CNX approach

The cause effect or Ishikawa diagram is shown in figure 5.7 that may influence the method performance criteria. Table 5.1 enlists the factors and their score that were considered in method development. Based on CNX risk assessment the contributing method parameters were divided into primary (High Risk, score ≥ 250) and secondary (marginal Risk, score $<$ 250) factors. pH and % organic in mobile phase were considered as primary factors due to high score. Other factors were screened by PBD to determine significant factors for optimization in CCD.

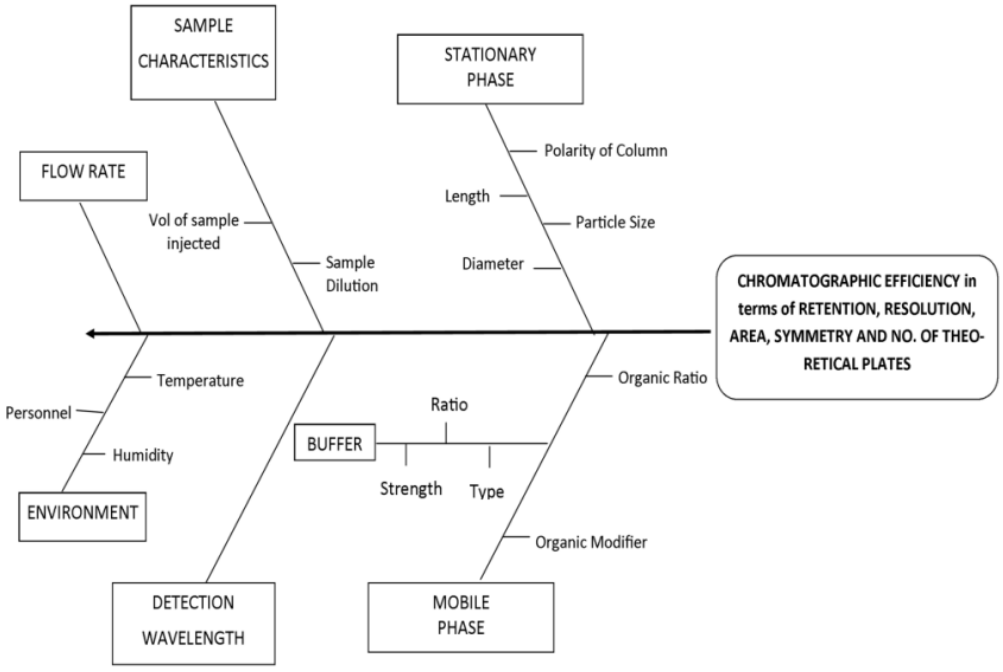

Figure 5.7: Ishikawa or cause effect diagram

Table 5.1: CNX risk assessment for chromatographic separation

Method parameter	Cause	Component attributes			Total score	C, N, X	Strategy
		Resolution	Retention time	Tailing			
	Attribute Score	**10**	**10**	**10**			
Column	Column age, of injection	10	10	10	300	N	New column
Column	Stationary phase type	10	10	10	300	C	C-18
Mobile Phase	pH	10	10	10	300	X	DoE
Mobile Phase	% organic	10	10	5	250	X	DoE
Mobile Phase	% MeOH	5	10	1	160	X	DoE
Column	Equilllibration	5	5	1	110	X	DoE
pump	Flow Rate	5	5	1	110	X	DoE
Instrumental	Wavelength	5	5	1	110	X	DoE
Mobile Phase	Buffer strength	1	5	1	70	X	DoE
Heater	Column Temp	1	5	1	70	X	DoE

Notes: C – controlled, N = Noise, E = Experimental; Scoring: 1 – negligible risk, 5 – low risk (potential impact), 10 – high risk (proven impact); Final score is the summation of each component attribute times the parameter score (eg:10X10+10X10+10X10=300)

5.4.2.2.3 PBD screening design

The matrix of PBD screening is presented in table 5.2 and some of the chromatographic trials of PBD screening are shown in figure 5.8. The half normal plot and pareto plot

(figure 5.9) showed that none of the factors are significant for response Rt and AS although % of methanol was most contributing factor. For response AREA again none of the factors were significant but flow rate was most contributing. For RS1 the significant factors were flow rate and wavelength. For RS2 flow rate was significant factor. So based on outcome of PBD screening flow rate was chosen for response surface optimization among secondary factors. Other contributing factor viz % of methanol was kept constant (10%) based on previous experience and analytical wavelength was fixed at 300 nm due to better absorption and sensitivity of DPs and CIO.

Table 5.2: Matrix of PBD screening with their measured responses.

	Independent Variable						Dependent Variable				
Run Order	FR	Temp.	WV	BS	Eq. Time	% MeOH	Rt	AS	AREA	RS1	RS2
1.	1.0	32.5	292.5	30	15	15	13.683	1.12	2560471	1.72	3.39
2.	1.2	40.0	280.0	50	20	0	14.567	1.01	1554993	1.10	1.87
3.	1.2	25.0	305.0	50	10	30	16.275	1.27	1259421	0.95	2.42
4.	1.0	32.5	292.5	30	15	15	13.683	1.42	2560471	1.72	3.39
5.	0.6	25.0	280.0	10	10	0	18.893	1.33	1906085	1.10	0.00
6.	1.2	25.0	305.0	10	10	0	9.960	1.16	1730125	1.71	3.18
7.	0.6	40.0	280.0	10	10	30	19.217	1.45	3447132	1.22	0.00
8.	0.6	40.0	305.0	50	10	30	15.646	1.34	1969993	1.15	2.76
9.	0.6	40.0	305.0	10	20	0	13.738	1.02	1439713	2.13	0.00
10.	0.6	25.0	305.0	50	20	0	17.210	1.34	3430420	2.31	0.65
11.	0.6	25.0	280.0	50	20	30	15.530	1.16	1335430	1.50	2.15
12.	1.2	25.0	280.0	10	20	30	22.632	1.40	1769993	3.00	3.40
13.	1.2	40.0	280.0	50	10	0	13.423	1.31	2101590	0.45	3.89
14.	1.2	40.0	305.0	10	20	30	25.927	1.33	326215	0.84	1.50

FR= flow rate, Temp.= temperature, WV=wavelength, BS= buffer strength, Eq. Time=equilibrium time, Rt= retention time of last eluting peak, AS=asymmetry, RS1= resolution between peak pair 1, RS2= resolution between peak pair 2.

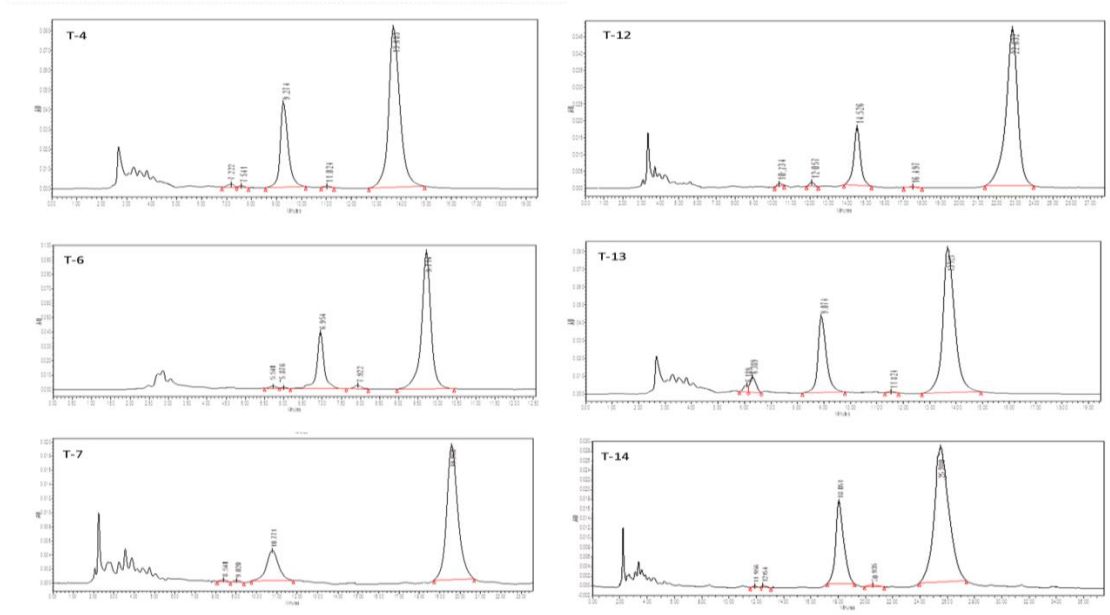

Figure 5.8: Some chromatograms of PBD screening

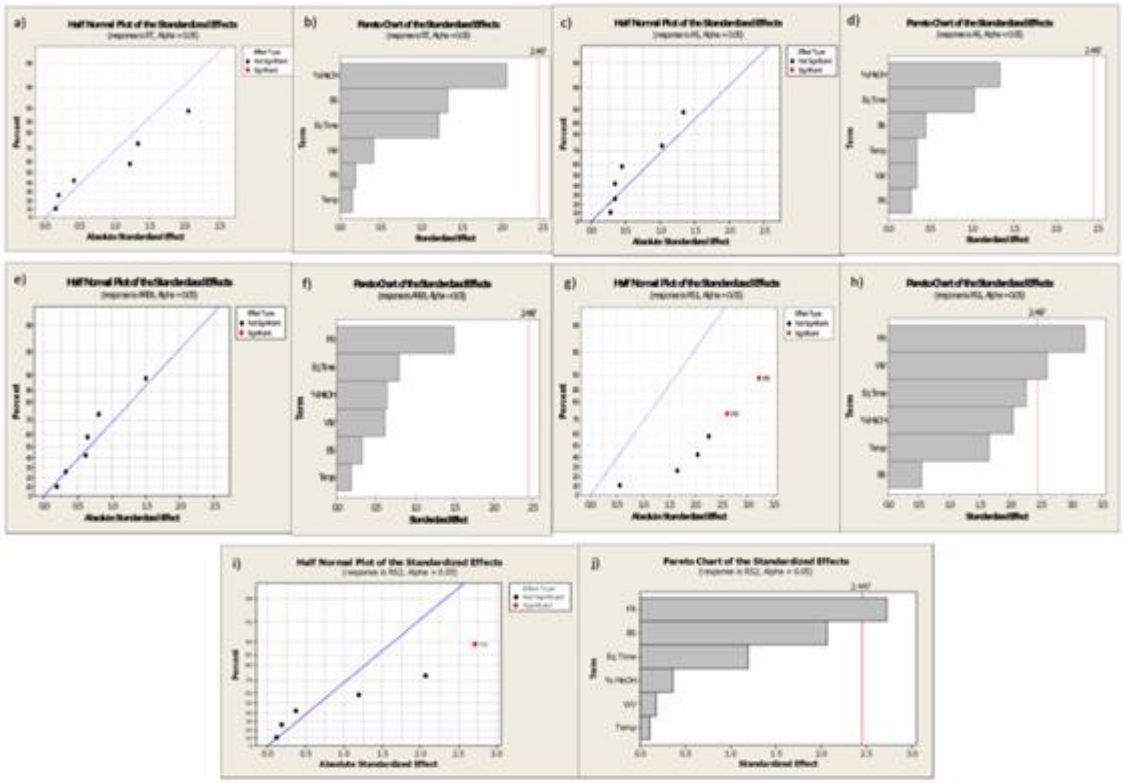

Figure 5.9: a) Half Normal plot for response Rt, b) Pareto plot for response Rt, c) Half Normal plot for response AS, d) Pareto plot for response AS, e) Half Normal plot for response AREA, f) Pareto plot for response AREA, g) Half Normal plot for response RS1, h) Pareto plot for response RS1, i) Half Normal plot for response RS2, j) Pareto plot for response RS2

5.4.2.2.4 CCD response surface design

Factors and their levels for CCD are shown in table 5.3. The matrix of CCD with their measured responses is shown in table 5.4. Some chromatograms of CCD trials are shown in figure 5.10.

Table 5.3: Variables and their levels for CCD

Factors	Coded Levels	Actual Levels
A: % Organic in Mobile Phase	-1	40
	1	60
B: pH of Mobile Phase	-1	4.2
	1	5.8
C: Flow Rate	-1	0.6
	1	1.2
Responses		Constraints
R1: Resolution between peak pair 1 (RS1)		1.5≤ R1≥2.5
R2: Resolution between peak pair 2 (RS2)		2≤ R1≥4
R3: Retention time of last eluting peak (Rt)		10 ≤ R1≥15
R4: Area of CIO (AREA)		12000 ≤ R1≥23000

Table 5.4: Matrix of experiments for CCD and results of the responses

	Independent Variable			Dependent Variable			
RUN	**ORG (A)**	**pH (B)**	**FR (C)**	**RS1**	**RS2**	**Rt**	**AREA**
1	40	4.2	0.6	3.36	4.55	22.48	1603817
2	60	5.8	1.2	1.32	2.24	4.45	2352450
3	40	5.8	0.6	4.86	4.3	21.83	1741020
4	50	5	0.9	0.58	2.61	9.94	1873768
5	60	4.2	0.6	1.28	1.61	8.23	2119245
6	40	5.8	1.2	4.03	4.07	15.27	1508537
7	50	6.34	0.9	0.4	3.16	10.71	2047112
8	50	5	0.9	0.58	2.61	9.94	1873768
9	40	4.2	1.2	3.27	4.58	15.38	1365030
10	50	5	0.9	0.58	2.61	9.94	1873768

11	50	5	0.9	0.58	2.61	9.94	1873768
12	50	5	0.9	0.58	2.61	9.94	1873768
13	60	4.2	1.2	1.23	1.9	5.5	1418660
14	60	5.8	0.6	0.74	1.82	8.1	2208076
15	33.18	5	0.9	5.04	4.52	36.42	1341020
16	50	3.65	0.9	1.28	2.99	9.68	1295398
17	50	5	0.39	4.16	3.28	14.13	2052450
18	50	5	1.40	1.33	2.98	7.33	1350180
19	50	5	0.9	0.58	2.61	9.94	1873768
20	66.81	5	0.9	0	0	5.5	1761430

ORG=% organic in mobile phase, pH=pH of mobile phase, FR= flow rate, Rt= retention time of last eluting peak, AS=asymmetry, RS1= resolution between peak pair 1, RS2= resolution between peak pair 2.

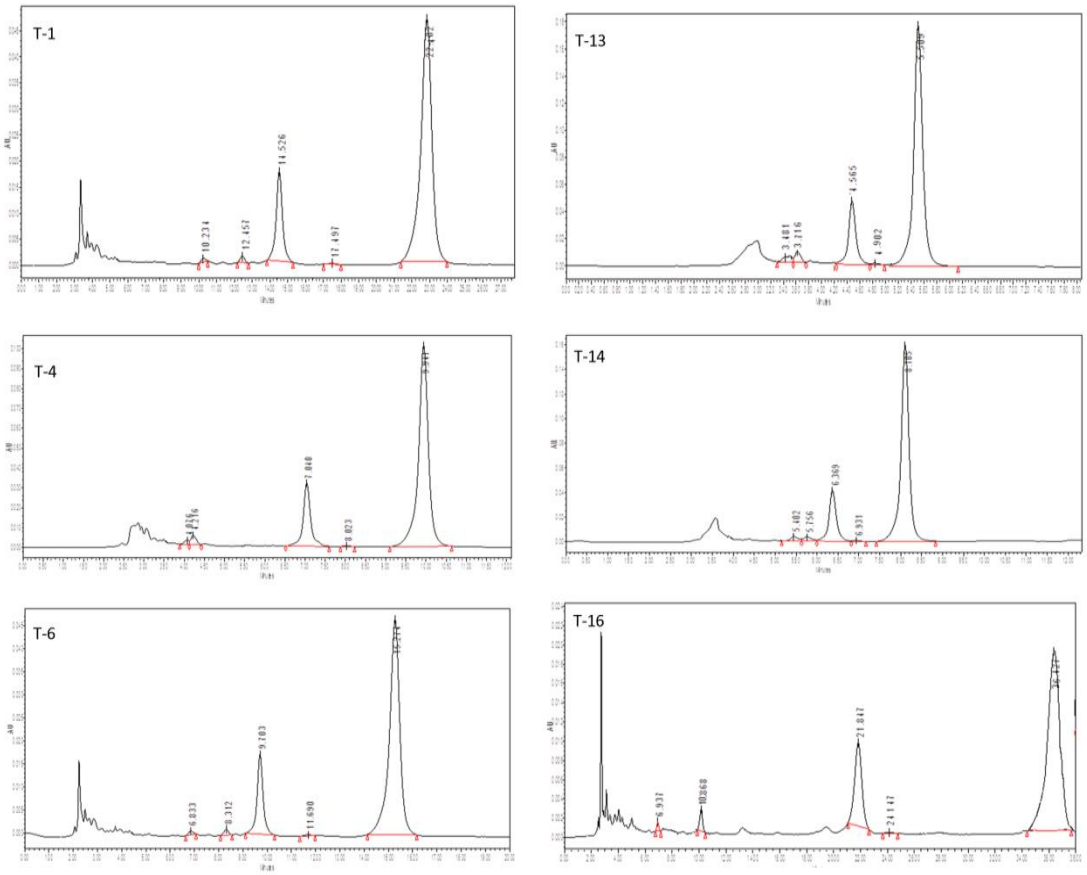

Figure 5.10: Some chromatograms of CCD Trials

Effect of factors on responses

RS1

Regression coefficients ANOVA results and of responses are presented in table 5.5 and 5.6. From regression analysis of reduced quadratic model it can be concluded that % of organic in mobile phase is most influencing factor affecting negatively for response RS1. The flow rate of mobile phase is also contributing negatively while pH of mobile phase is not contributing significantly. The same can be inferred from main and interaction plots for RS1 (figure 5.11) and contour and 3D plots (figure 5.12).

The quadratic equation in terms of coded factors for reduced model is as follows:

RS1 = +0.71-1.42*A-0.38 * C+0.18 * AC+0.75 * A^2 +0.83 * C^2

Table 5.5: Regression analysis results

Factors	RS1 coefficient	p value (prob>F)	RS2 coefficient	p value (prob>F)	Rt coefficient	p value (prob>F)	AREA coefficient	p value (prob>F)
Intercept	+0.71	< 0.0001	+2.60	< 0.0001	+9.80	< 0.0001	+1.770E+006	0.0001
A	-1.42	< 0.0001*	-1.28	< 0.0001*	-7.37	< 0.0001*	+1.894E+005	0.0013*
B	--	--	+5.558E-003	0.9237	--	--	+1.880E	0.0013*
C	-0.38	0.0352*	+4.000E-004	0.9945	-2.30	0.0002*	-1.617E+005	0.0042*
AB	--	--	+0.16	0.0511	--	--	--	--
AC	+0.18	0.4056	+0.11	0.1548	+0.91	0.1621	--	--
BC	--	--	-0.016	0.8304	--	--	--	--
A^2	+0.75	0.0003	-0.061	0.2969	+3.59	< 0.0001	--	--
B^2	--	--	+0.23	0.0020	--	--	--	--
C^2	+0.83	0.0001	+0.25	0.0012	-0.024	0.9582	--	--

Regression coefficients are in coded values, *Statistically significant ($p<0.05$)

Table 5.6: ANOVA results showing the effect of independent variables on the responses

Response	Model	SS	DF	MS	F-value	p-value	PRESS	r^2	Adj-r^2	Pred-r^2	AP
RS1	RQM	46.56	5	9.31	26.05	< 0.0001	16.77	0.9030	0.8683	0.6749	14.611
RS2	FQM	24.46	9	2.72	62.21	< 0.0001	3.33	0.9825	0.9667	0.8661	29.214
RT	RQM	1011.04	5	202.21	66.50	< 0.0001	179.31	0.9596	0.9452	0.8298	29.063
AREA	RLM	1.330E+012	3	4.433E+011	13.79	0.0001	9.043E+011	0.7212	0.6689	0.5097	13.450

RQM=reduced quadratic model, FQM= full quadratic model, RLM= reduced linear model, SS= Sum of Squares, DF= Degrees of freedom, PRESS= prediction error sum of squares, Pred- r^2= Predicted r^2, Adj- r^2= Adjusted r^2, , AP= Adequate Precision.

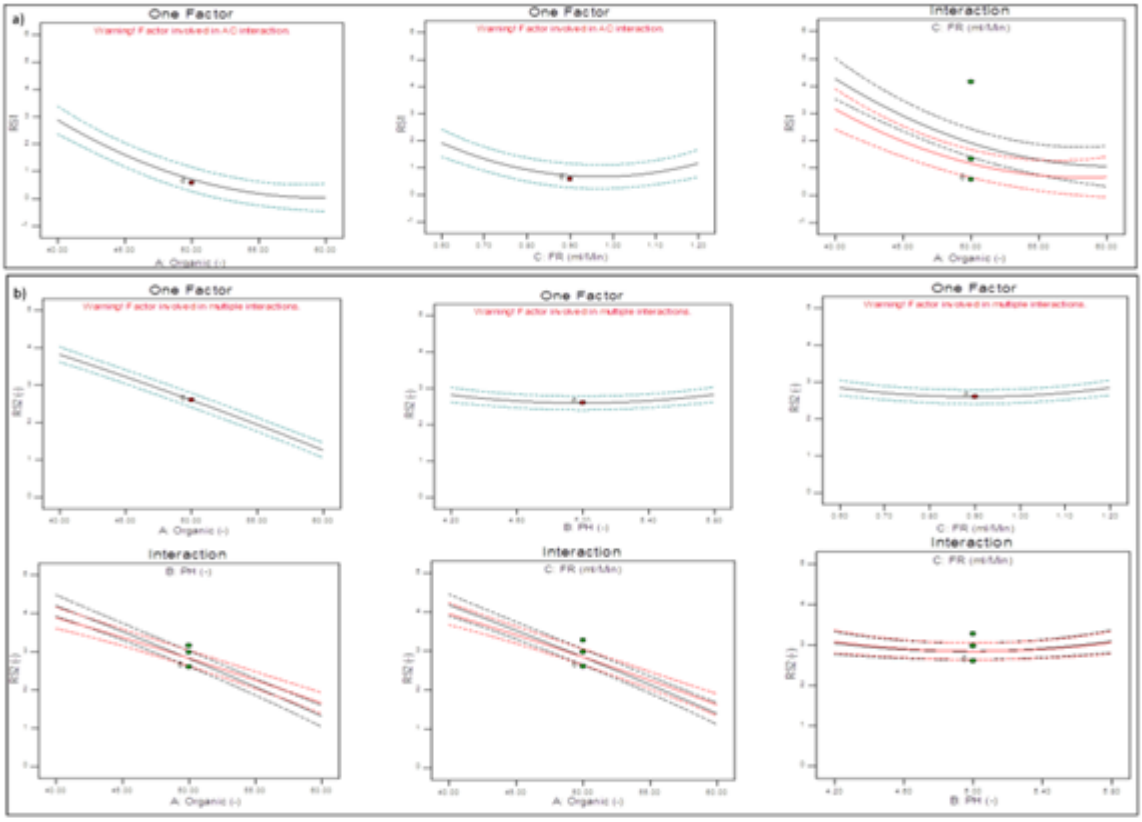

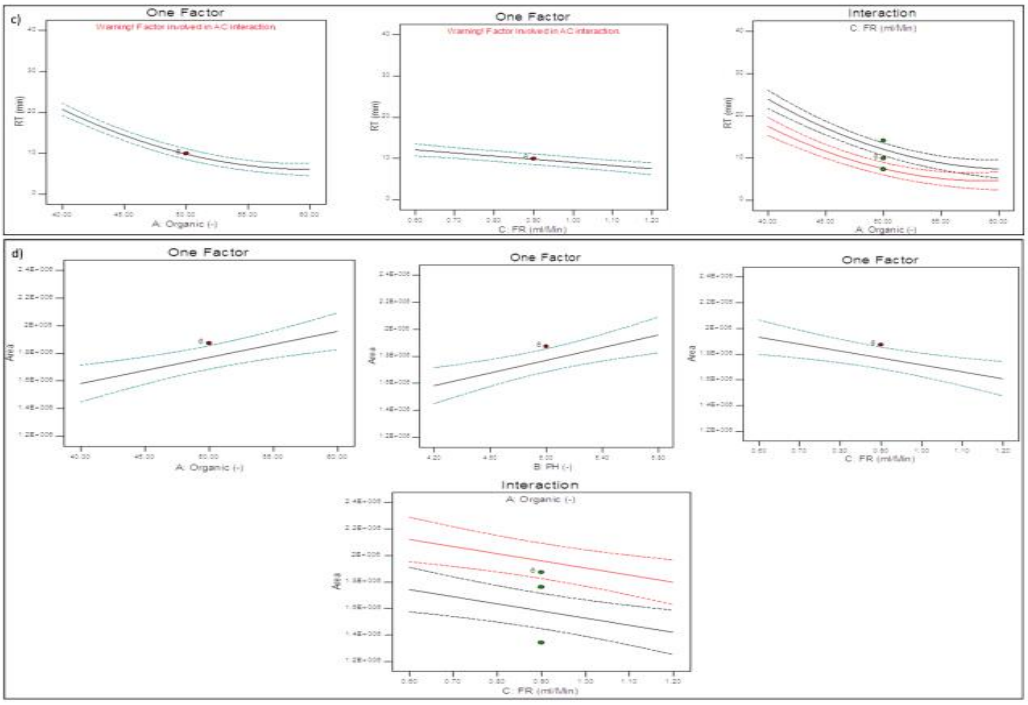

Figure 5.11: Main and interaction effect plots for a) RS1, b) RS2, c) Rt and d) AREA

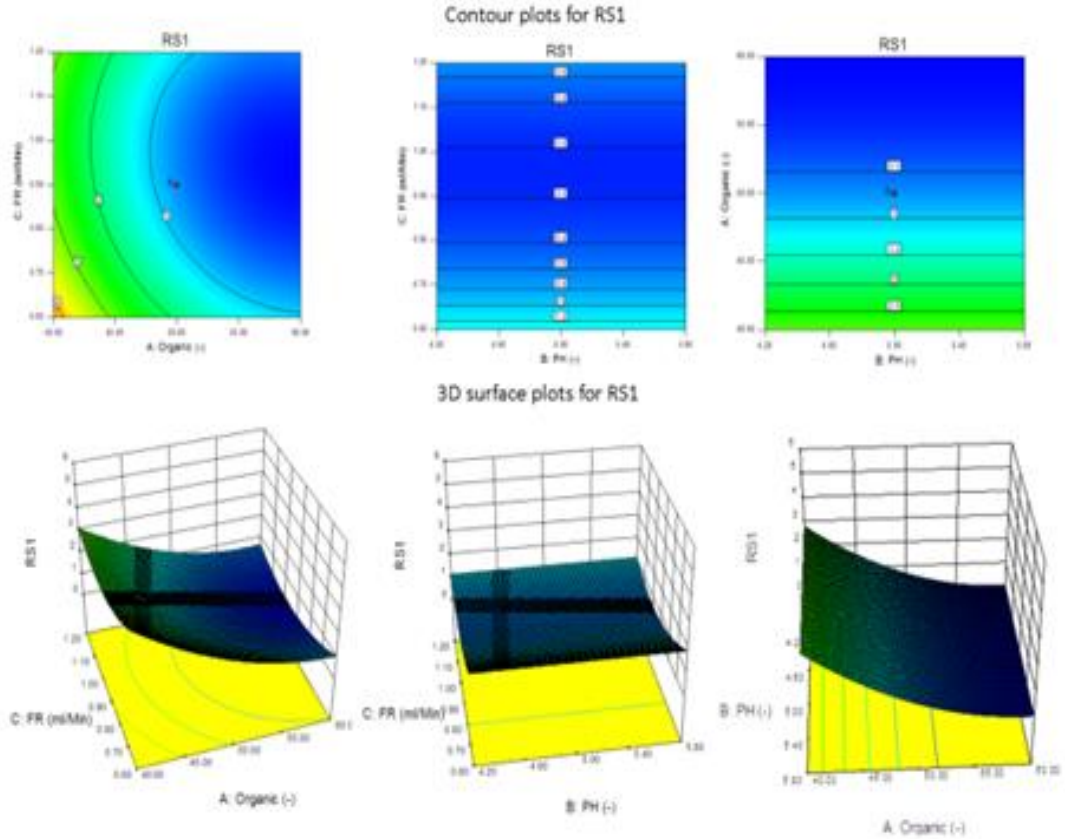

Contour plots for RS2

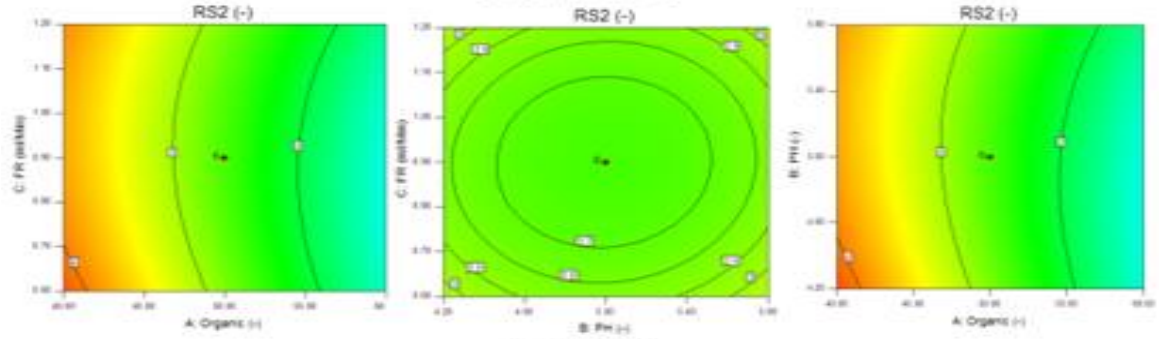

3D plots for RS2

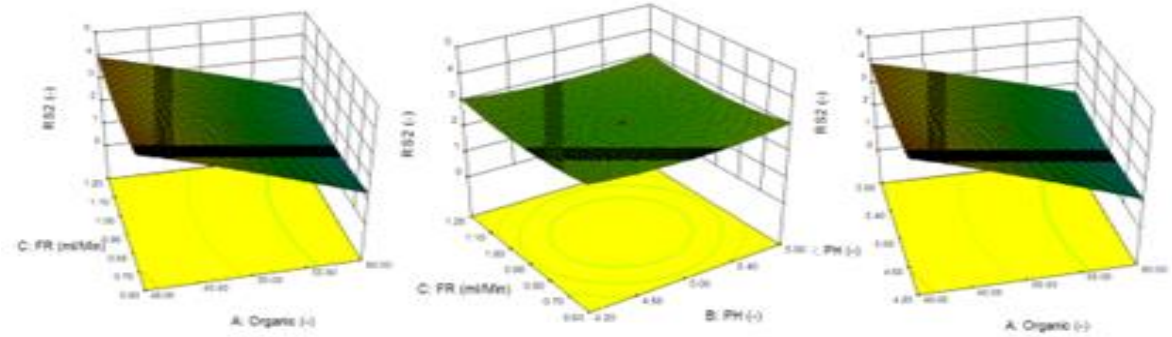

Contour plots for RT

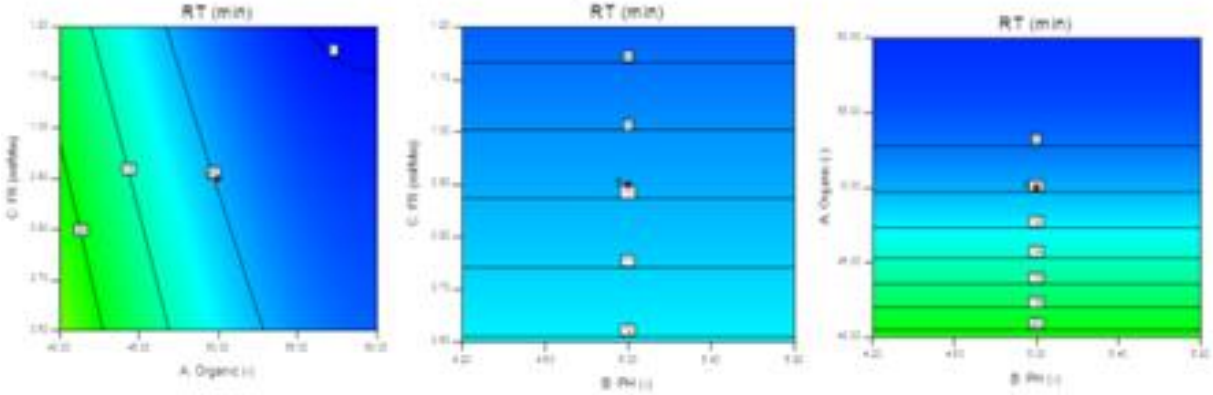

3D plots for RT

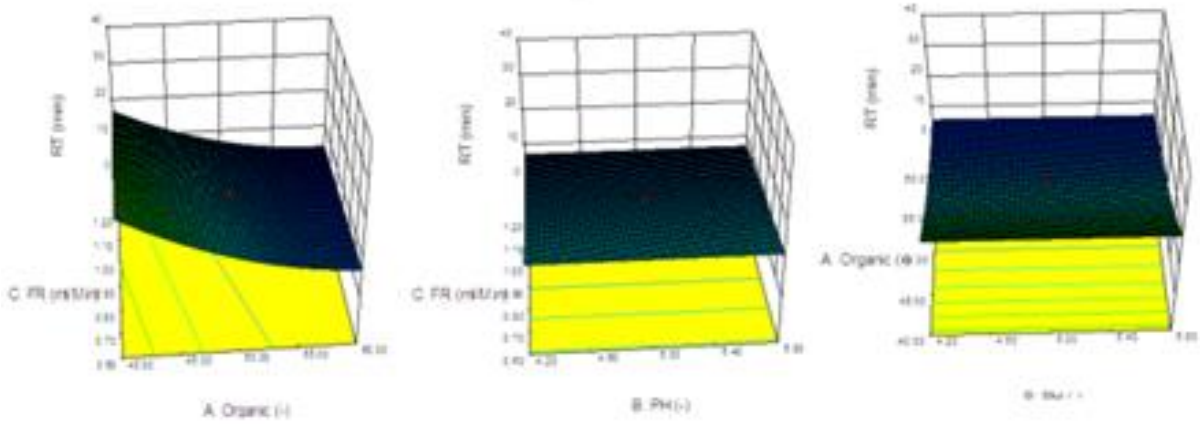

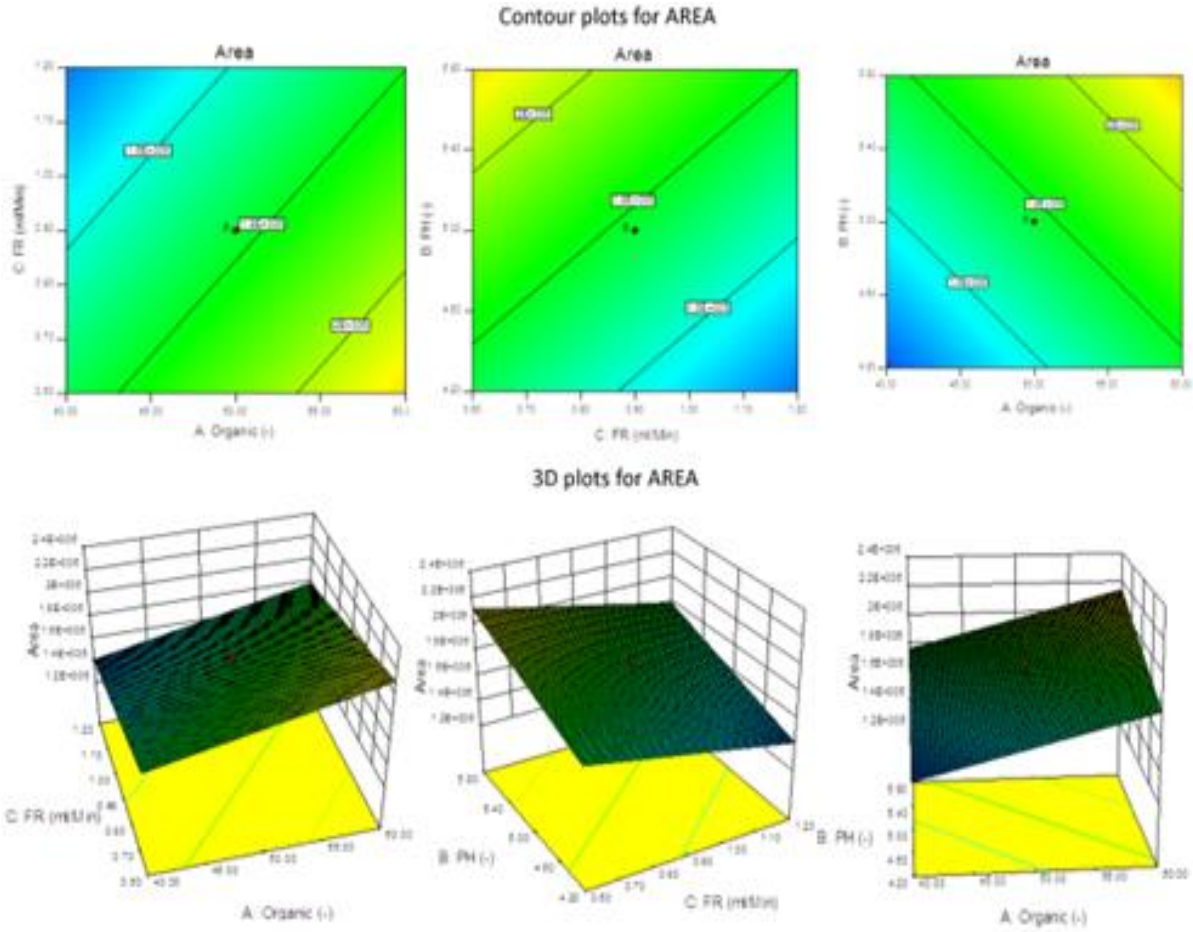

Figure 5.12: Contour and 3D Plots for a) RS1, b) RS2, c) Rt and d) AREA (value increases from blue to green)

RS2

From table 5.5 and figure 5.11 it can be concluded that % of organic in mobile phase is most influencing factor affecting negatively response RS2. pH and flow rate of mobile phase are not contributing significantly as the associated p-value are more than 0.05, but these terms are included in model to support hierarchy.

The quadratic equation in terms of coded factors for full model is as follows:

RS2 = +2.60 -1.28 * A +5.558E-003 * B +4.000E-004 * C +0.16 * AB +0.11 * AC -0.016 * BC -0.061 * A^2 +0.23 * B^2 +0.25 * C^2

Rt

As shown in table 5.5 and figure 5.11 it can be concluded that % of organic in mobile phase is most influencing factor affecting negatively response Rt. The flow rate of mobile

phase is also contributing negatively while pH of mobile phase is not contributing significantly.

The quadratic equation in terms of coded factors for reduced model is as follows:

RT = +9.80 -7.37* A -2.30* C +0.91* AC +3.59* A^2 -0.024* C^2

AREA

As shown in table 5.5 and figure 5.11 % of organic in mobile phase and pH of mobile phase are contributing positively and significantly with same magnitude (having same p-value). Also flow rate of mobile phase is contributing significantly and negatively influencing the response AREA.

The linear equation in terms of coded factors for reduced model is as follows:

Area= +1.770E+006 +1.894E+005* A +1.880E+005* B -1.617E+005* C

Model Fitting and Statistics

Statistically, high values of the r^2 for all dependent variables indicate a good model fit. The reasonable good agreement of adjusted and predicted r^2 values, especially for reduced models signifies good model fit (table 5.6). Better Predicted-r^2 obtained for reduced model might be due to exclusion of insignificant terms. Further full and reduced model, showed the adequate precision value more than 4, that indicates adequate model discrimination.

Interaction between the factors and residual plots

The ANOVA results (table 5.6) and figure 5.11 depicts the interaction effects amongst the factors. The p-value indicates that there is no interaction effects among the factors, as the associated p-value for interactions are more than 0.05. The residual plots such as normal probability plot of residuals and residual versus run for RS1, RS2, Rt and AREA are depicted in figure 5.13 The normal probability plot of residuals for responses indicates that the residuals appear to follow almost straight line and hence non-normality, outliers, skewness or unidentified variables does not exist. The plot of residual versus fit of all responses reveals that residuals appear to be scattered about zero and hence it can be stated that missing terms, non-constant variance, outliers or influential points does not exist in selected model.

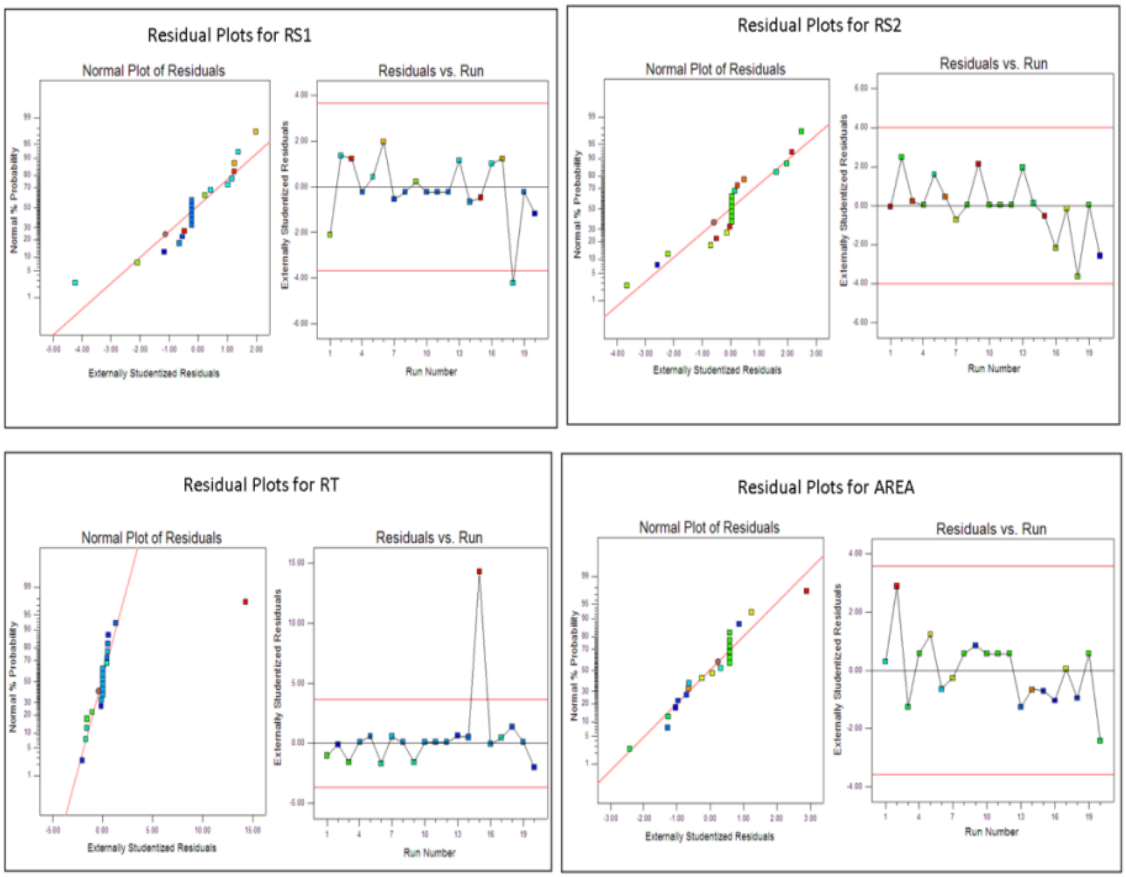

Figure 5.13: Residual plots for RS1, RS2, Rt and AREA

Evaluation of model using cross-validation

Five experiments were conducted to evaluate the reliability of the model, by varying the variables at values other than that of the model. Low values of % bias indicate the validity of selected model. Table 5.7 shows the predicted, experimental values and % bias for responses. Percent relative error or Bias between predicted and experimental values for responses were calculated by the equation:

$$\text{Bias} = \frac{(\text{Predicted Value} - \text{Experimental Value})}{\text{Predicted value}}$$

Table 5.7: % Bias of responses for the cross validation set

Responses	Test	Factors/Levels			Predicted values	Experimental Values	Bias (%)
		A	B	C			
RS1	1	44.50	4.48	0.9	1.70	1.5	0.11764706
	2	45.00	4.60	0.8	1.66	1.59	0.04216867
	3	46.00	5.70	1.1	1.50	1.7	-0.13333333
	4	47.00	5.50	0.7	1.58	1.69	-0.06962025
	5	46.50	5.15	0.7	1.82	1.78	0.02197802
RS2	1	44.50	4.48	0.9	3.41	3.5	-0.02639296
	2	45.00	4.60	0.8	3.28	3	0.08536585
	3	46.00	5.70	1.1	3.30	2.9	0.12121212
	4	47.00	5.50	0.7	3.07	3.3	-0.07491857
	5	46.50	5.15	0.7	3.13	3.5	-0.11821086
Rt	1	44.50	4.48	0.9	14.857	14.1	0.05095241
	2	45.00	4.60	0.8	14.56	13.9	0.04532967
	3	46.00	5.70	1.1	11.17	12.9	-0.15487914
	4	47.00	5.50	0.7	13.15	12.7	0.03422053
	5	46.50	5.15	0.7	14.21	12.9	0.0921886
AREA	1	44.50	4.48	0.9	1559366	1408537	0.09672457
	2	45.00	4.60	0.8	1629277	1761430	-0.08111144
	3	46.00	5.70	1.1	1741266	1773768	-0.01866573
	4	47.00	5.50	0.7	1935867	2052450	-0.06022263
	5	46.50	5.15	0.7	1840144	2003817	-0.08894576

Optimization using desirability function

The optimized methods with acceptable ranges for responses were determined by setting the goals of the critical responses. Response RS1 was selected to be in between 1.5-2.5, response RS2 was set to be in between 2-4, response Rt was set to be in between 10-15 in

order to reduce the total run time of method and AREA were set to be in between 12000-23000. Desirability function was calculated for the responses. Several optimized solutions for the specified criteria were generated by the software; out of which 4 solutions were used for checkpoint analysis (n=4) as shown in table 5.8. One of the solutions with % of organic in mobile phase 44, pH 5.6 flow rate 1.1 was chosen as the optimized working point as it gives acceptable separation with reasonable symmetric peak shape and peak purity. The peak purity studies of resolved peaks are presented in table 5.10. The desirability and overlay plot for optimized working point is shown in figure 5.14. The observed responses values (table 5.9) lie within 95% confidence interval of the predicted response values.

Table 5.8: Point Verification and working point selection

Optimized solution	Pred RS1	Obs RS1	Pred RS2	Obs RS2	Pred Rt	Obs Rt	Pred AREA	Obs AREA
%ORG: 51, pH:5.74, FR: 0.6	1.72	1.69	2.90	3.0	11.10	11.6	2129437	2208076
%ORG: 44, pH:5.23, FR: 0.9	1.73	1.70	3.31	3.4	14.70	14.1	1679764	1695398
%ORG: 48, pH:4.32, FR: 0.6	2.0	1.91	3.24	3.2	13.64	13.0	1722480	1761430
%ORG: 44, pH:5.6, FR: 1.1	**2.25**	**2.0**	**3.63**	**3.4**	**13.41**	**12.7**	**1650914**	**1723768**

RS1=Resolution between peak pair 1, RS2= Resolution between peak pair 2, Rt=Retention time

Table 5.9: Observed versus Predicted responses for optimized working point

Response	Prediction	Observed	SE Mean	95% CI low	95% CI high
R1	**2.25**	**2.0**	0.257408	1.50405	2.60822
R2	**3.63**	**3.4**	0.0861943	3.21953	3.60364
RT	**13.41**	**12.7**	0.750761	10.9495	14.1699
AREA	**1650914**	**1723768**	56263	1539934	1778477

CI=Confidence interval, SE=Standard error

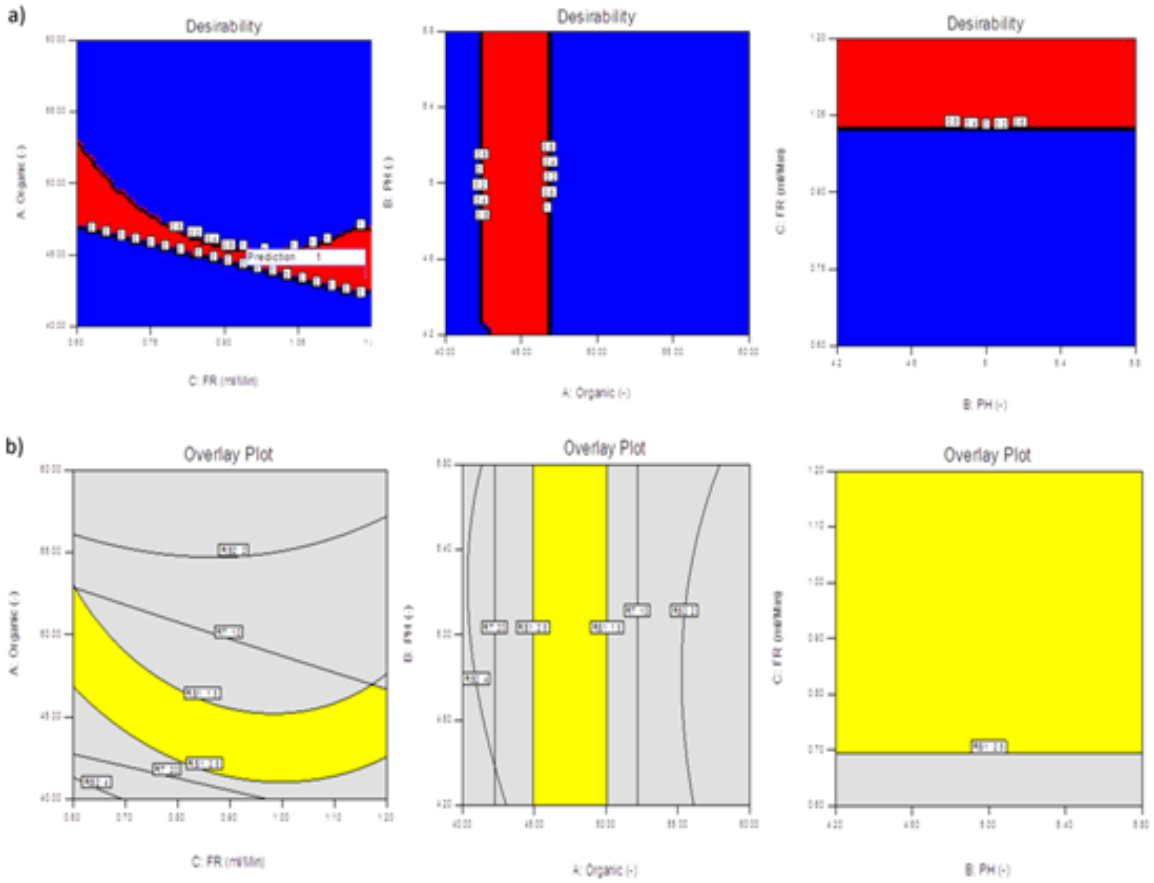

Figure 5.14: Desirability (desirability increases from blue to red region; blue region indicates 0 and red region indicates 1 desirability) and overlay plot (yellow region: design space, gray region: undesirable region) for optimized chromatogram

The final optimized chromatogram obtained with the selected working point is depicted in figure 5.15 that comprises of well resolved pairs of CIO and DPs. The peak purity studies of resolved peaks in mixture of degradants were also carried out and are shown in table 5.10 and figure 5.16. During peak purity analysis it was observed that peak for DP-3 did not passes the peak purity test while other peaks in the chromatogram (i. e. peaks of DP-1, DP-2 and DP-4) were pure. Later on LC-MS/MS studies revealed that the peak of DP-3 was mixture of two peaks and showed two different masses.

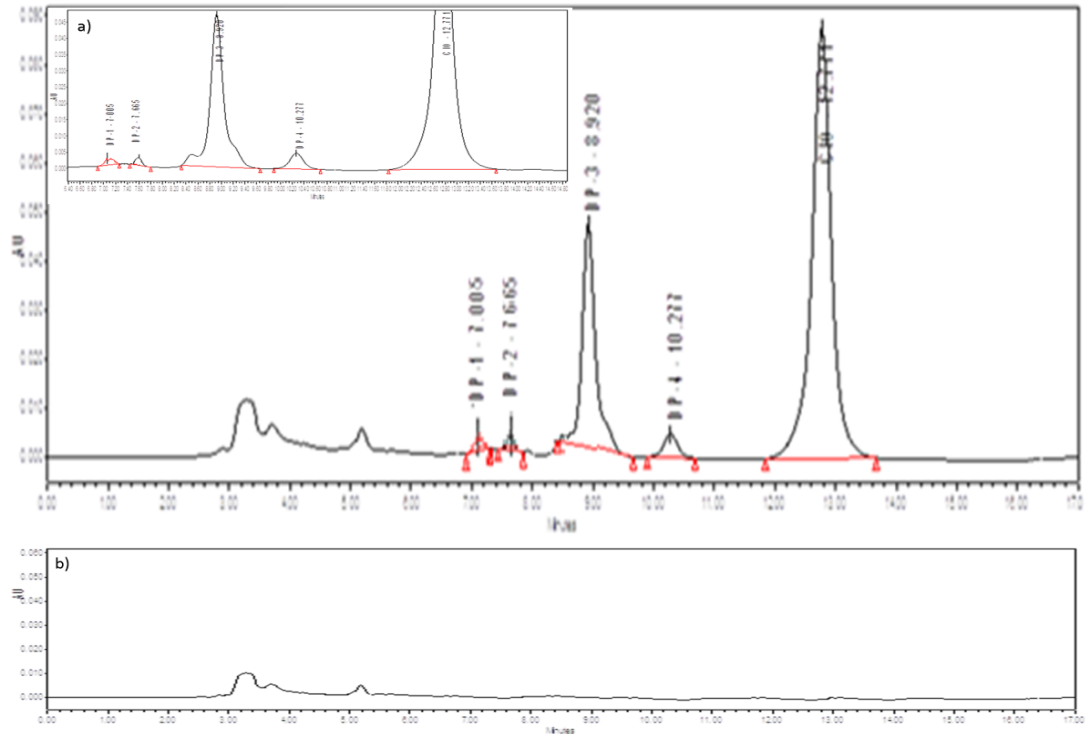

Figure 5.15: a) Chromatogram showing resolved peaks in mixture of degradants b) Blank chromatogram

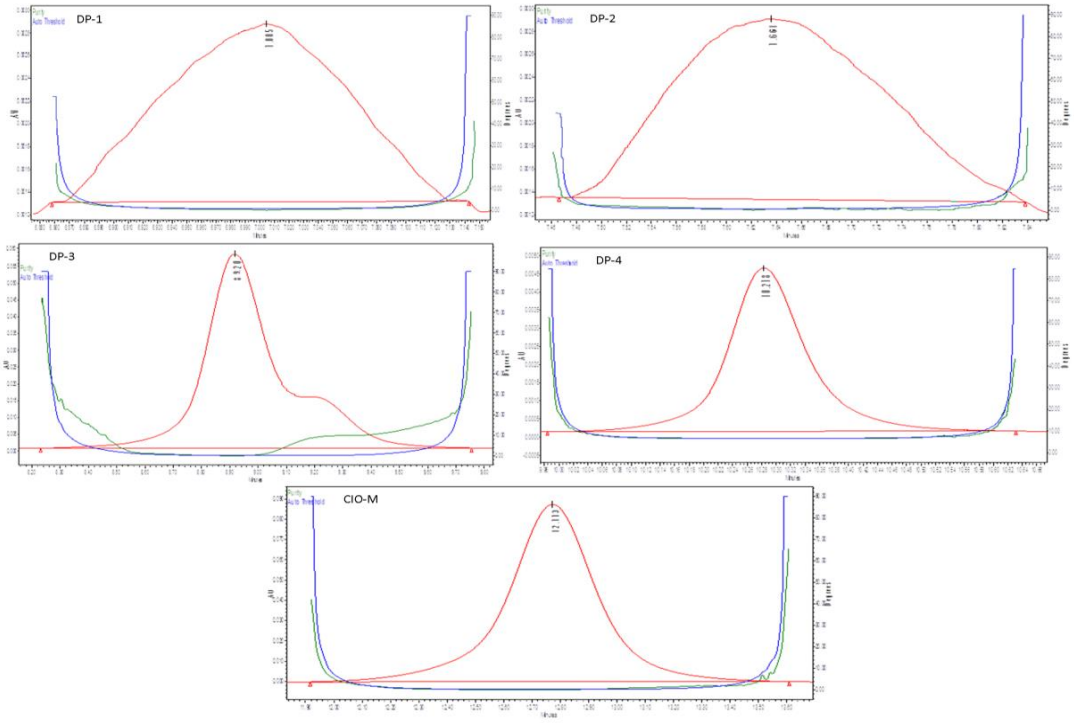

Figure 5.16: Peak purity plots for optimized chromatographic conditions

Table 5.10: Peak purity studies for peaks of optimized chromatographic conditions

S. No.	Peaks	Rt	Peak Purity Angle	Peak purity Threshold
1.	DP-1	7.00	2.220	2.505
2.	DP-2	7.66	1.626	1.650
3.	DP-3*	8.91	0.964	0.719
4.	DP-4	10.27	0.302	0.544
5.	CIO	12.77	0.256	0.261

Note: *indicates peaks are not pure; Peak at Rt 8.44 was observed as shouldered peak which gives two different masses in LC-MS

5.4.2.3 Method Validation using ICH Q2(R1) guideline and total error approach

5.4.2.3.1 Linearity and Range

To determine linearity, test solutions of CIO were prepared from stock solution of drug, 1 mg/ml in mobile phase at concentration levels of 20-120 µg/ml in triplicate. The linearity of the method was established in accordance with ICH Q2(R1) guideline. To construct calibration curve concentrations of CIO were plotted against peak areas; the response was linear in the selected concentration range with R^2 value 0.9999. Overlay chromatogram and linearity plot is shown in figure 5.17.

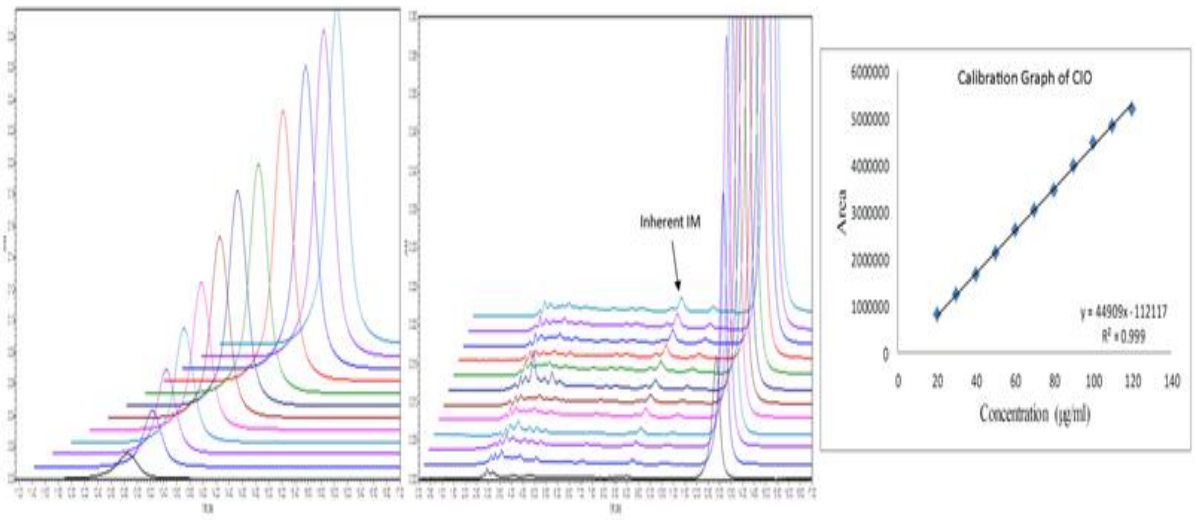

Figure 5.17: Overlay chromatogram and calibration graph of CIO

5.4.2.3.2 Response function (calibration curve)

Linear regression model was used to prepare calibration curves in the present method. The validation and calibration sets used for model generation were shown in table 5.11 and 5.12. To study response function three different sets were prepared within the concentration range of 20-120 µg/ml. All three sets were found to follow the linear regression model. The regression analysis studies revealed that series 3 showed the best coefficient of determination with r^2 0.9999 and was selected for further studies.

Table 5.11: Validation standards

Sample ID	Series	Conc. Level (µg/ml)	Introduced conc. (µg/ml)	Analytical response (Area)
A1	1	1	20	789918
A10	1	4	80	3177912
A11	1	4	80	3165209
A12	1	4	80	3180432
A13	1	5	100	3939473
A14	1	5	100	3933100
A15	1	5	100	3946173
A16	1	6	120	4720374
A17	1	6	120	4731162
A18	1	6	120	4732916
A2	1	1	20	788572
A3	1	1	20	792726
A4	1	2	40	1561196
A5	1	2	40	1594066
A6	1	2	40	1569014
A7	1	3	60	2369171
A8	1	3	60	2367114
A9	1	3	60	2375348
B1	2	1	20	784208
B10	2	4	80	3147103
B11	2	4	80	3149010
B12	2	4	80	3175398
B13	2	5	100	3996392
B14	2	5	100	3941931
B15	2	5	100	4005719
B16	2	6	120	4713128
B17	2	6	120	4709641
B18	2	6	120	4730415

B2	2	1	20	791074
B3	2	1	20	789702
B4	2	2	40	1571979
B5	2	2	40	1585903
B6	2	2	40	1549695
B7	2	3	60	2362035
B8	2	3	60	2370990
B9	2	3	60	2364887
C1	3	1	20	789926
C10	3	4	80	3148019
C11	3	4	80	3181947
C12	3	4	80	3150592
C13	3	5	100	3933979
C14	3	5	100	4012097
C15	3	5	100	3950748
C16	3	6	120	4719832
C17	3	6	120	4729169
C18	3	6	120	4737095
C2	3	1	20	786788
C3	3	1	20	791002
C4	3	2	40	1581979
C5	3	2	40	1599862
C6	3	2	40	1576929
C7	3	3	60	2365390
C8	3	3	60	2370989
C9	3	3	60	2377183

Table 5.12: Calibration standards

Sample ID	Series	Conc Level (µgm/ml)	Introduced conc (µgm/ml)	Analytical response (Area)
A1	1	1	20	790141
A2	1	1	20	794395
A3	1	2	60	2369171
A4	1	2	60	2375348
A5	1	3	120	4727298
A6	1	3	120	4732916
B1	2	1	20	788042
B2	2	1	20	792874
B3	2	2	60	2371367
B4	2	2	60	2376974

B5	2	3	120	4729128
B6	2	3	120	4734015
C1	3	1	20	780086
C2	3	1	20	794722
C3	3	2	60	2370989
C4	3	2	60	2377183
C5	3	3	120	4729169
C6	3	3	120	4737095

Furthermore in order to check whether the regression model for calibration was adequate, a test of lack of fit (LOF) and Levene's test (i. e. evaluation of homogeneity of variance) were performed. As demonstrated in table 5.13 outliers were not found in calibration curve, since the p-values were found to be higher than 0.05. Standard residual plot was also plotted as shown in table 5.14 and figure 5.18. Back calculation was done to conform the chosen regression equation. Linear plot (figure 5.19) was generated between nominal and back calculated concentration based upon absolute β-expectation limit, which shows r^2 value 0.9998 with equation Y = 0.07876 + 1.002 X where Y = Back calculated concentrations in µg/ml and X = Introduced concentration in µg/ml.

Table 5.13: LOF and Levene's test for linear regression model

Test	**Error**	**SS**	**df**	**MS**	**F_{calc}**	**F_{crit} 95%**	**p-value**
Lack of Fit	LOF error	1.9315E+08	3	6.4384E+07	2.405	3.863	0.1348
	Pure error	2.4094E+08	9	2.6771E+07			
Levene's	Model	3.3996E+06	2	1.6998E+06	0.6954	3.682	0.5143
	Error	3.6667E+07	15	2.4445E+06			

SS= sum of square,df= degrees of freedom, MS=mean square

Table 5.14: Standardized residual from the selected calibration model

Sample ID	Series	Conc. level	Introduced conc.	Analytical response	Fitted value	Standardized residual
A1	1	1	20	790141.0	7.9418E+05	0.9343
A2	1	1	20	794395.0	7.9418E+05	0.04856
A3	1	2	60	2369171.0	2.3691E+06	0.02453
A4	1	2	60	2375348.0	2.3691E+06	1.452
A5	1	3	120	4727298.0	4.7314E+06	0.9442
A6	1	3	120	4732916.0	4.7314E+06	0.3538
B1	2	1	20	788042.0	7.9333E+05	1.013
B2	2	1	20	792874.0	7.9333E+05	0.08677
B3	2	2	60	2371367.0	2.3694E+06	0.3791
B4	2	2	60	2376974.0	2.3694E+06	1.454
B5	2	3	120	4729128.0	4.7335E+06	0.8351
B6	2	3	120	4734015.0	4.7335E+06	0.1018
C1	3	1	20	780086.0	7.9072E+05	1.344
C2	3	1	20	794722.0	7.9072E+05	0.5064
C3	3	2	60	2370989.0	2.3686E+06	0.3063
C4	3	2	60	2377183.0	2.3686E+06	1.089
C5	3	3	120	4729169.0	4.7353E+06	0.7801
C6	3	3	120	4737095.0	4.7353E+06	0.2218

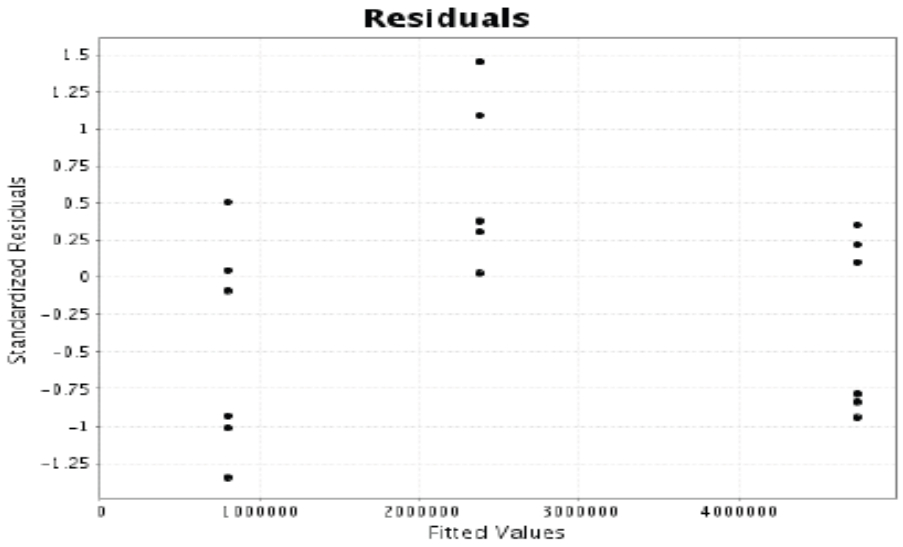

Figure 5.18: Standard residual plot of three different series representing absence of outliers

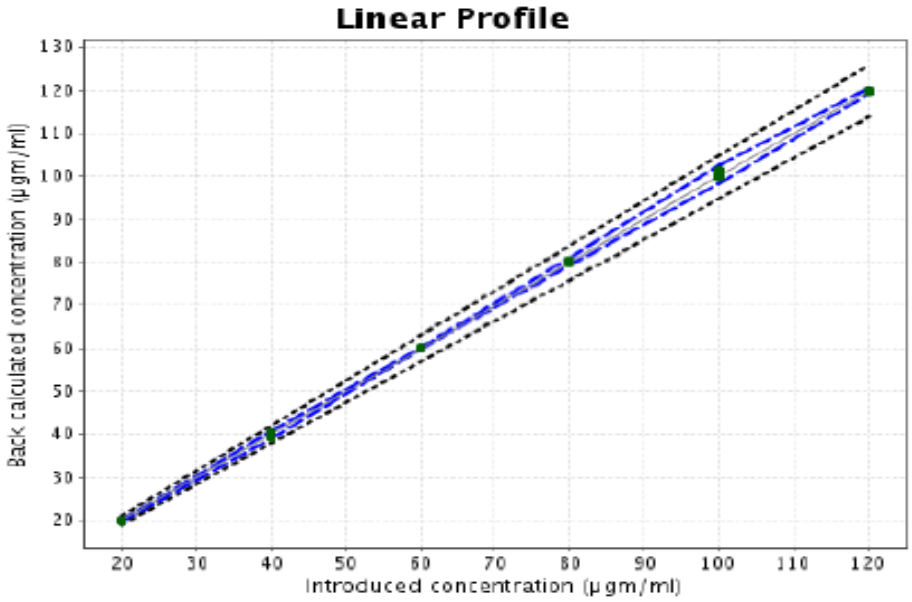

Figure 5.19: Plot of linear regression model of back calculated concentrations versus the introduced concentrations. (plain line = identity line (Y = X); Dashed line = Accuracy Profile; dotted curves = the acceptance limits. The method is considered to be valid within the range for which the dashed curves lie within dotted acceptance limits.)

5.4.2.3.3 Trueness

The percentage relative bias of the method was calculated to justify the trueness of the method. As shown in table 5.15 it can be concluded that the trueness for all concentrations is acceptable, since the percentage relative bias is limited between -0.4339 % to 0.4289 %, furthermore its percentage recovery lies within 95% confidence interval.

Table 5.15: Results of trueness study

Conc. Level	Mean introduced conc. (µg/ml)	Mean Back calculated conc. (µg/ml)	Absolute Bias (µg/ml)	Relative Bias (%)	Recocery (%)	95% confidence interval of recovery (%)
1	20	19.91	-0.08677	-0.4339	99.57	[99.29 , 99.84]
2	40	39.89	-0.1051	-0.2629	99.74	[98.95 , 100.5]
3	60	60.01	0.005756	0.009593	100.0	[99.84 , 100.2]
4	80	80.17	0.1732	0.2164	100.2	[99.84 , 100.6]
5	100	100.4	0.4289	0.4289	100.4	[99.80 , 101.1]
6	120	119.8	-0.2168	-0.1807	99.82	[99.66 , 99.98]

5.4.2.3.4 Precision

The % RSD of for both repeatability and intermediate precision were found to be less than 2%; these suggest the reproducibility of developed analytical method. The results of relative and absolute intermediate precision and repeatability are shown in table 5.16. Further 95% confidence upper limit have also been demonstrated.

Table 5.16: Results of absolute and relative intermediate precision and repeatability

Conc. (µg/ml)	Relative intermediate precision and repeatability				Absolute intermediate precision and repeatability		
	Rep (%RSD)	IP (%RSD)	95% Upper confidence limit		Rep (SD)	IP (SD)	Ratio of variance components (Between/ within)
			Rep (SD) (µg/mL)	IP (%RSD)			
20	0.3474	0.3633	0.1331	0.2107	0.06948	0.07267	0.09386

40	1.019	1.034	0.7807	1.151	0.4076	0.4137	0.02995
60	0.2101	0.2188	0.2415	0.3782	0.1261	0.1313	0.08368
80	0.4751	0.4974	0.7280	1.155	0.3801	0.3979	0.09611
100	0.7914	0.8253	1.516	2.383	0.7914	0.8253	0.08739
120	0.1909	0.2075	0.4388	0.7550	0.2291	0.2490	0.1810

Rep= Repetability, IP= Intermediate Precision, SD= Standard Deviation, RSD= Relative Standard Deviation

5.4.2.3.5 Accuracy

Standard addition method was utilized to evaluate the accuracy of the method in formulation matrix. The accuracy obtained by considering linear regression model has been presented in table 5.17. It was also found that the β-expectation tolerance limits did not exceed the acceptance limit which indicates that 95% of β-percent of the future determination of unknown samples will be included within the tolerance limits and is shown by accuracy profile (figure 5.20). Accuracy profile of the method was also justified by risk profile (figure 5.21) by choosing maximum risk level at 5.0%. It indicates that the risks of outliers are with in the limits and also future analysis of unknown sample will be in range.

Table 5.17: Result of accuracy study in terms of risk assessment and relative beta-expectation tolerance limit obtained by linear regression model

Matrix	**Conc. Level (%)**	**Conc. (µg/ml)**	**Beta expectation tolerance limits (µg/ml)**	**Relative Beta expectation tolerance limits (%)**	**Risk (%)**
Lotion	80	20	[19.73 , 20.09]	[-1.341, 0.4735]	0.000351
	100	60	[59.68 , 60.33]	[-0.5354, 0.5546]	0.000007
	120	100	[98.37 , 102.5]	[-1.629, 2.487]	0.07405

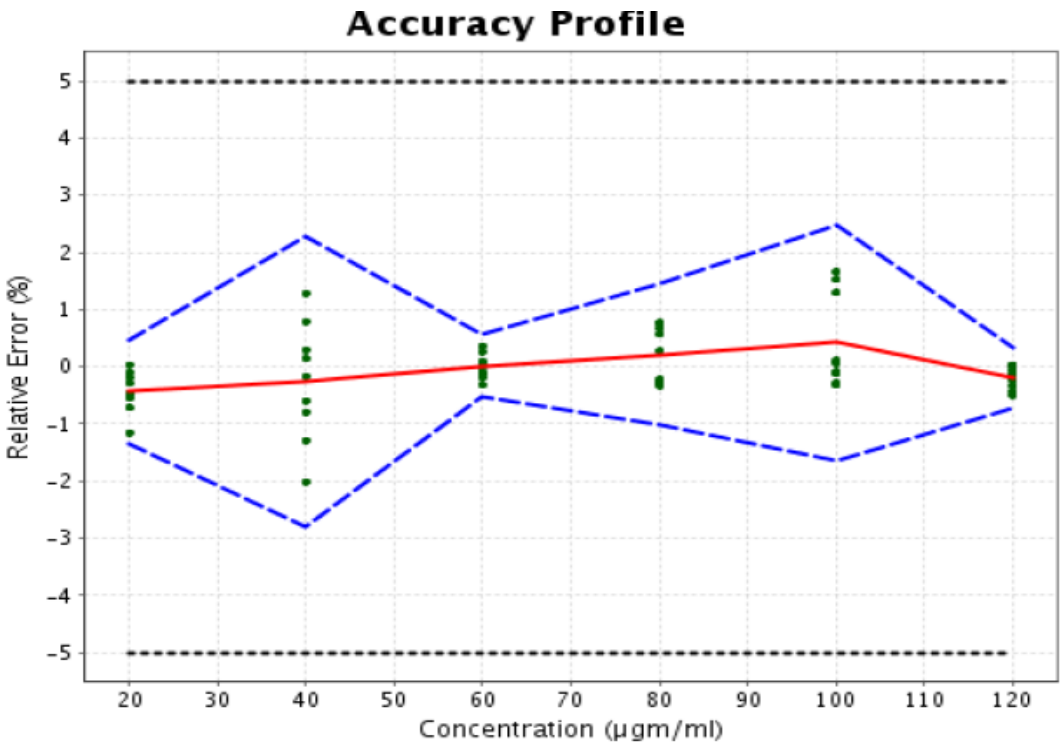

Figure 5.20: Accuracy profile obtained by considering Linear Regression (plain red line = the relative bias, the dashed lines = β-expectation tolerance limits; the dotted lines = the acceptance limits; dots = relative error of the back calculated concentrations that is plotted against targeted concentration)

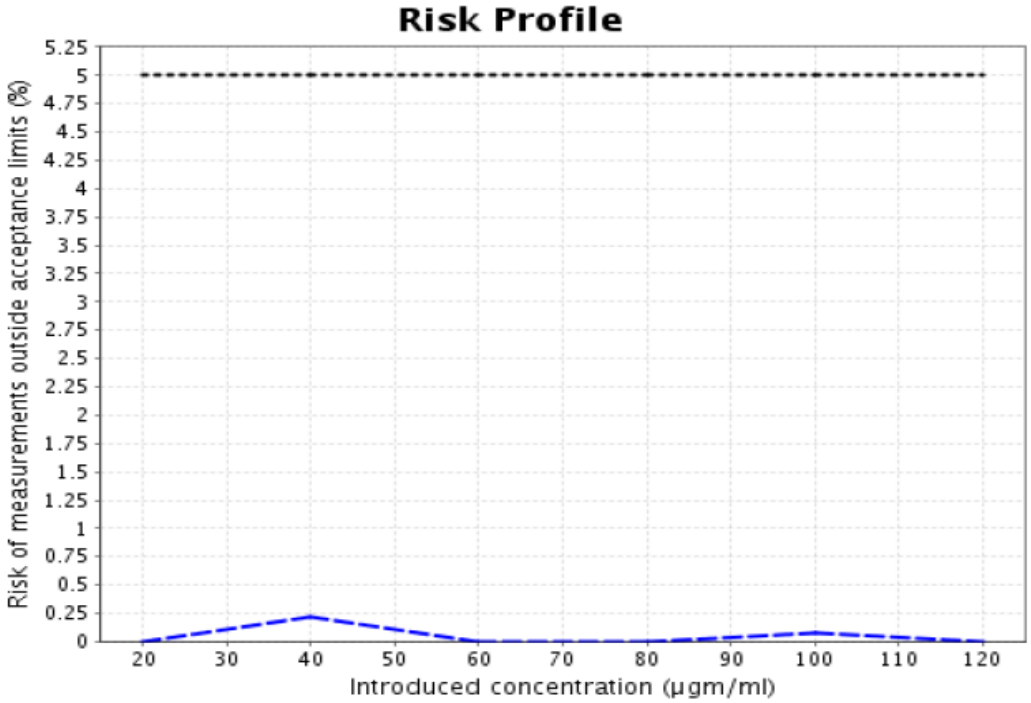

Figure 5.21: Risk profile obtained by considering Linear Regression (dotted line = the maximum risk level chosen, 5.0 %.)

5.4.2.3.6 Limit of detection and quantification

The LOD and LOQ of method were found to be 0.6247 and 1.8732 µg/ml, respectively. This indicates the sensitivity of developed method to analyze the marketed formulations.

5.4.2.3.7 Robustness studies

Small but deliberate changes in the % of organic in mobile phase, pH and flow rate were made to study the robustness of the developed method and were determined in the form of percentage RSD. Table 5.18 represented the results of robustness study, showing the effect of variation on area, Rt, tailing factor and theoretical plates.

Table 5.18: Results of robustness study

Chromatographic changes	Area (% RSD)	Rt (% RSD)	Tailing Factor (% RSD)	Theoretical plates (% RSD)
		Organic Ratio		
44	1.21	1.09	0.84	0.96
46	1.00	0.98	0.78	0.89
48	1.42	1.43	0.81	0.91
		pH		
4.2	0.76	0.90	0.43	0.76
4.4	0.71	0.87	0.44	0.70
4.6	0.78	0.93	0.42	0.73
		Flow Rate (ml/min)		
0.8	0.77	0.98	0.38	0.91
1.0	0.51	0.79	0.35	0.80
1.2	0.85	0.91	0.41	0.94

5.4.2.4 Uncertainty of Measurment

The uncertainty, uncertainty of bias, expanded uncertainty and relative expanded uncertainty was calculated for the present method. From table 5.19 it can be concluded that the uncertainty values fall within limit so, there is no doubt that the developed method is robust.

Table 5.19: Results of uncertainty of measurements

Conc. (µg/ml)	Uncertainty (µg/ml)	Conc. Level (µg/ml)	Uncertainty of the Bias (µg/ml)	Expanded Uncertainty (µg/ml)	Relative Expanded Uncertainty (µg/ml)
20	0.07725	1	0.02622	0.1545	0.7725
40	0.4373	2	0.1418	0.8746	2.186
60	0.1394	3	0.04701	0.2788	0.4647
80	0.4231	4	0.1438	0.8462	1.058
100	0.8769	5	0.2964	1.754	1.754
120	0.2664	6	0.09486	0.5329	0.4441

5.4.2.5 Stress degradation studies

As presented in figure 5.15 four DPs were formed under stress conditions. The summary of forced degradation condition with % degradation (% Deg) in various conditions is presented in table 5.20. The % Deg was calculated by the formula:

$$\%\,Deg = \frac{\left[\begin{array}{l}(\text{Initial area of untreated stock solution}\\ -\text{reduced area of treated stock solution})\end{array}\right]}{\text{Actual initial area of untreated stock solution}} \times 100$$

CIO was stable under neutral, dry heat induced, and thermal-humidity degradation conditions. The drug is most sensitive under UV light. Furthermore it is susceptible to oxidative degradation. Degradation under acid and base hydrolysis was observed by refluxing the drug with acid or alkali for longer time. The chromatograms of stressed samples are shown in figure 5.21.

Table 5.20: Summary of stress degradation of CIO API and formulation

Stressor Type	Stressor Conc.	Time	% Deg (API)	% Deg (Formulation)

Acid degradation	1N HCl at 80^0C	12 hr	47.51	47.24
Base degradation	0.5N NaOH at 80^0C	10 hr	30.34	29.99
Neutral degradation	100 ^{0}C	12 hr	No degradation	
Oxidative degradation	6% H_2O_2 at 80^0C	6 hr	50.98	50.80
Photolytic degradation	5382 LUX and 144UW/cm^2	21 days	63.85	62.23
Dry Heat induced degradation	80º C	21 days	No degradation	
Thermal Humidity induced degradation	40 º C 70 ± 5% RH	21 days	No degradation	

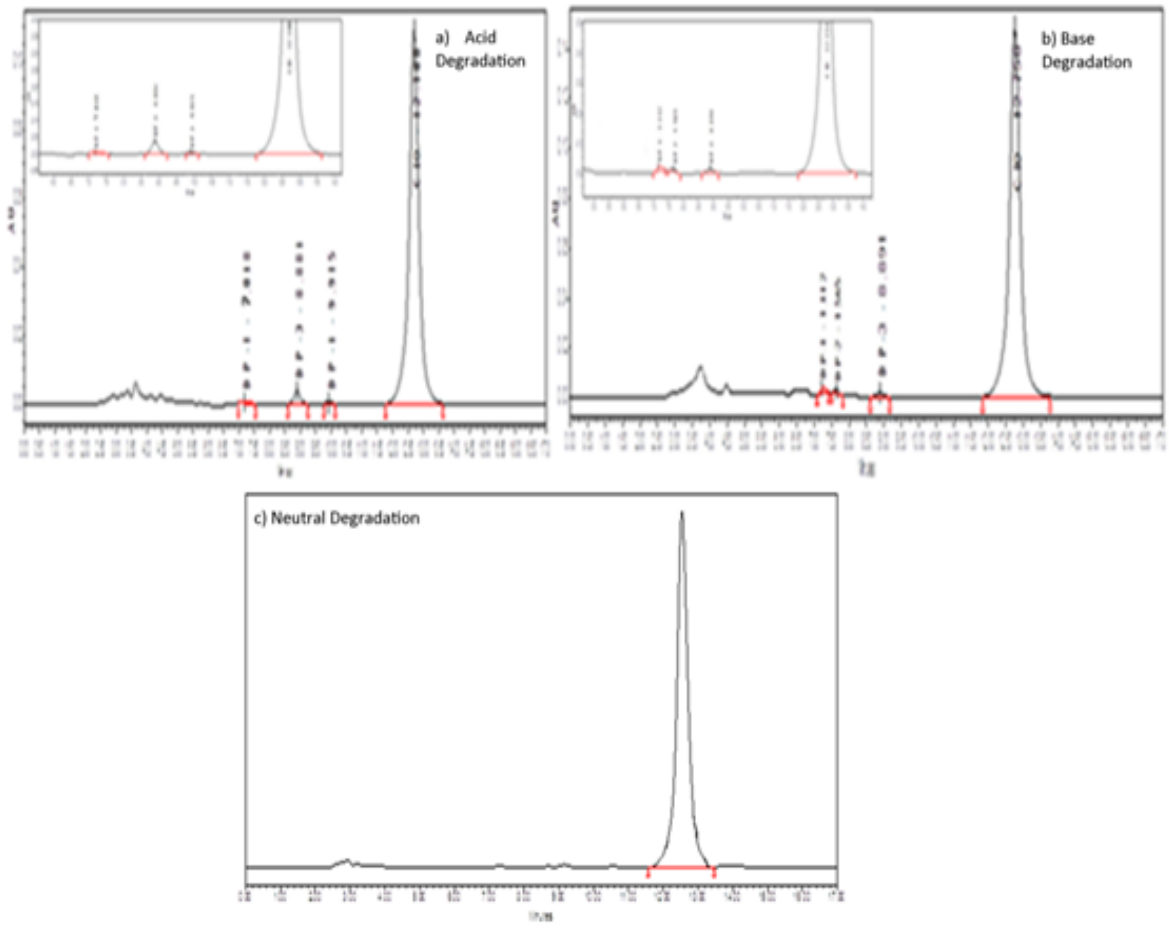

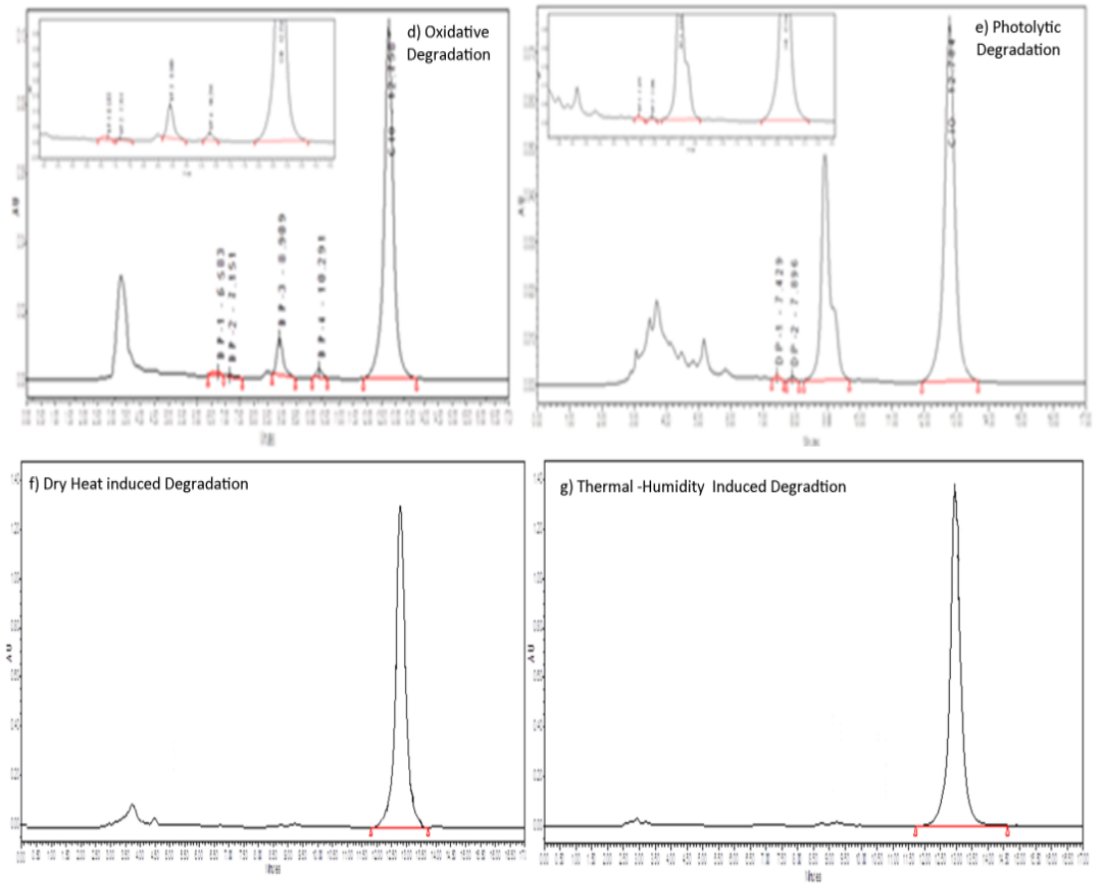

Figure 5.22: Chromatograms of a) acid degradation, b) base degradation, c) Neutral degradation, d) oxidative degradation e) Photolytic degradation, f) Dry heat induced degradation and g) Thermal-Humidity induced degradation

5.4.2.6 Applicability of developed stability indicating assay method for analysis of formulation

The developed method was used to analyze stress degraded samples of a formulation containing CIO. Stress degradation were carried out under same condition as specified for CIO and analyzed in the same way by same chromatographic condition. The DPs were discernible and well separated. As presented in table minor variation was observed in degradation of API and formulation.

5.5 SECTION –B

DEGRADATION KINETIC STUDY OF PIDOTIMOD BY HPLC METHOD

Degradation kinetic was studied for oxidative and photolytic degradation as CIO was comparatively more stable towards acid and base degradation.

5.5.1 EXPERIMENTAL

5.5.1.1 Chemicals and Reagents

The chemicals and reagents utilized in present section were same as described in section 3.4.1.1.

5.5.1.2 Equipments and Chromatographic Condition

The equipments utilized in this section were same as described in section 3.4.1.2 and chromatographic conditions were same as described in section 5.4.1.2.

5.5.1.3 Preparation of Stock, Sample and Buffer solutions

Standard and stock solutions were prepared in same solvent with same dilutions as described in section 5.4.1.3. For preparation of sample solutions 10 mg of CIO was dissolved with variable strength of H_2O_2 (30%, 15% and 6%) to study kinetics of oxidative degradation. These solutions were transferred into another clean and dry round bottom flask and refluxed in a thermostatically controlled oil bath at specified temperatures (60, 80 and 100^0C). For photolytic degradation 1 mg/ml solution of CIO was prepared in ACN and kept in photostability chamber. Aliquots of 0.5 ml of the sample solutions were withdrawn at different time intervals, derivatized as per method b described in section 5.4.1.3, diluted with mobile phase to make the final concentration C_0 = 110 µg/ml and filtered through 0.2 µm membrane filter before HPLC analysis. The % of drug Degradation (% Deg) was calculated from the formula:

$$\%\,Deg = \frac{\left[\begin{array}{l}(\text{Initial area of untreated stock solution}\\ -\text{reduced area of treated stock solution})\end{array}\right]}{\text{Actual initial area of untreated stock solution}} \times 100$$

5.5.2 RESULTS AND DISCUSSION

The degradation rate kinetics were determined using linear regression analysis by plotting % of drug degradation (% Deg) versus time (for zero-order process), log of % Deg versus time (for first-order process) and 1/% Deg Versus time (for second-order process). Each experiment was done in triplicate, and average values were taken for the analysis. Also, the arrhenius plots (plot of log of the rate constant versus the reciprocal of the temperature) were constructed to study the effect of temperature on the rate of oxidation. The rate constant (K_{obs}), half-life ($t_{1/2)}$ and activation energy (Ea) were also calculated from the slope of lines at each temperature of oxidative degradation process.

5.5.2.1 Kinetics of oxidative degradation

The regression equation and r^2 value for zero, first and second order reaction for oxidative degradation are presented in table 5.21. The oxidative degradation followed first order kinetics as r^2 value is highest in all conditions. In order to demonstrate the effect of temperature on the rate constant the arrhenius plot was constructed. Finally after studying different parameters that affected the rate of the reaction it was concluded that the rate of oxidation is directly proportional to temperature and strength of stressor. Reaction kinetic plots and arrhenius plots are shown in figure 5.22 and 5.23. The half- life and activation energy at different concentration and temperature are shown in table 5.22.

Table 5.21: Regression equation and r^2 value for zero, first and second order reaction for oxidative degradation

S. No	Conc. (H_2O_2)	r^2 Value				Regression Equation		
		Temp.	Zero Order	First Order	Second Order	Zero Order	First Order	Second Order
1	30%	60	0.9602	0.9891	0.9431	8.1984x - 1.2577	0.1395x + 0.8867	-0.0148x + 0.1007
		80	0.9602	0.9836	0.9706	7.8758x + 5.0689	0.1084x + 1.0949	-0.0087x + 0.0671
		100	0.9839	0.9908	0.9531	9.4392x + 8.7729	0.1033x + 1.2247	-0.0066x + 0.0512
2	15%	60	0.8874	0.9929	0.9312	7.6346x - 5.0113	0.1606x + 0.6884	-0.0229x + 0.148

		80	0.9497	0.9904	0.9413	7.3502x + 1.3136	0.1241x + 0.9467	-0.0128x + 0.0916
		100	0.9813	0.9891	0.9342	6.7464x + 7.0242	0.1008x + 1.1004	-0.0088x + 0.0689
		60	0.8199	0.9893	0.8153	8.4992x - 14.309	0.2985x - 0.1298	-0.1187x + 0.6371
3	6%	80	0.8739	0.9888	0.9217	8.7912x - 12.665	0.2483x + 0.1933	-0.0606x + 0.3441
		100	0.8855	0.9901	0.8909	9.388x - 12.633	0.2354x + 0.3076	-0.0495x + 0.2823

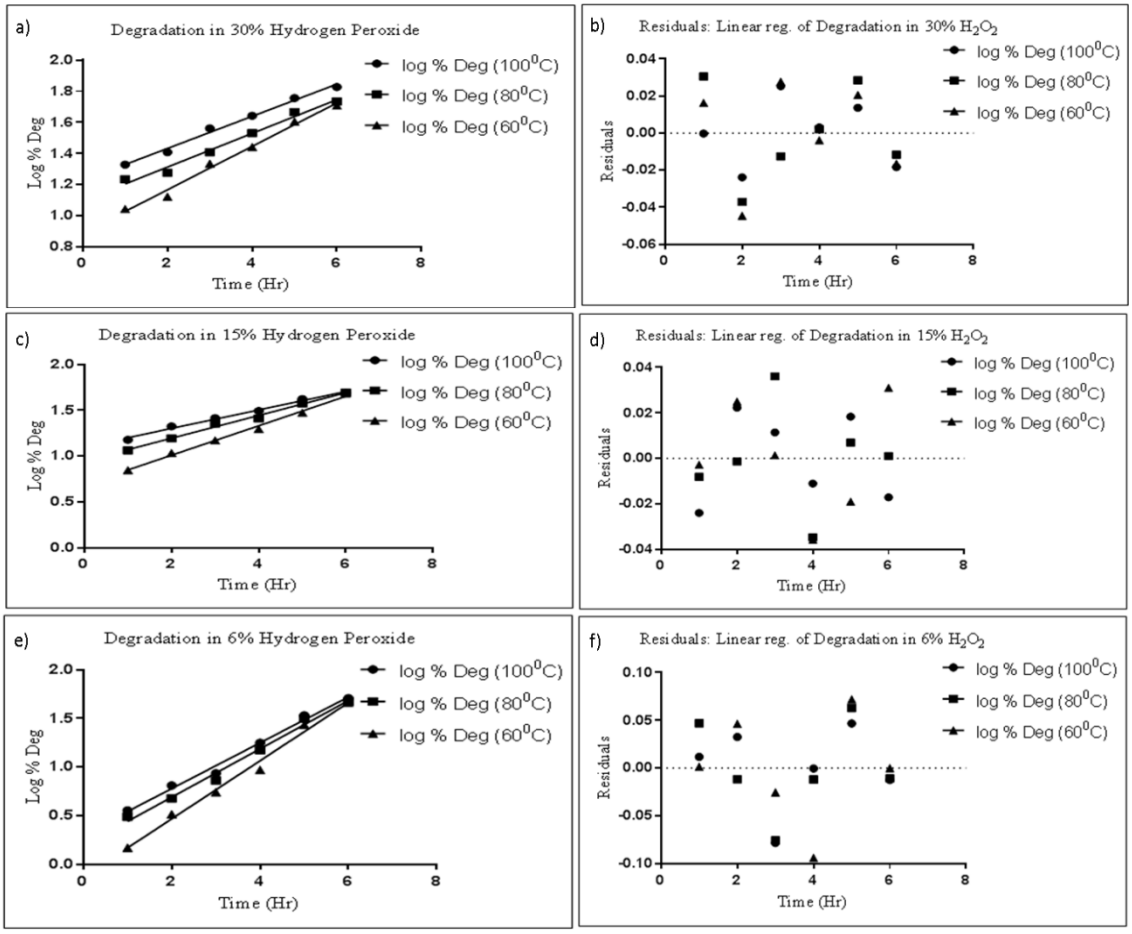

Figure 5.23 : First order reaction kinetic and residual plots for oxidative degradation

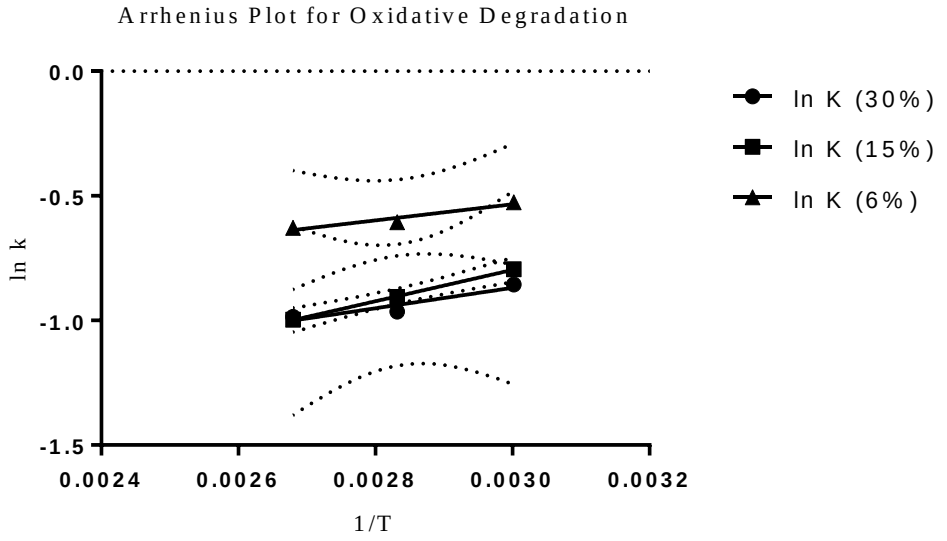

Figure 5.24: Arrhenius plot for oxidative degradation

Table 5.22: Half- life ($t_{1/2}$) and activation energy (Ea) for first order reaction kinetic

S. No	Conc. (H_2O_2)	Temp.	$t_{1/2}$ (min)	Ea (kj/mol)
1		60	4.9677	
	30%	80	6.3929	3.4110
		100	6.7086	
2		60	4.3150	
	15%	80	5.5842	5.2320
		100	6.8750	
3		60	2.3216	
	6%	80	2.7909	2.6899
		100	2.9439	

5.5.2.2 Kinetics of photolytic degradation

The r^2 values for photolytic degradation indicate that this conditions followed zero order reaction kinetics (figure 5.25) as r^2 values are highest (almost near to one) for zero order degradation reaction. The regression equation and r^2 value for zero, first and second order

reaction for photolytic degradation is shown in table 5.23. The rate of degradation increases with the increase in time for photolytic degradation.

Table 5.23: Regression equation and r^2 value for zero, first and second order reaction for photolytic degradation

S. No	r^2 Value			Regression Equation		
	Zero Order	First Order	Second Order	Zero Order	First Order	Second Order
1	0.9909	0.9028	0.6982	4.0135x - 17.583	0.0636x + 0.5993	-0.0077x + 0.1537

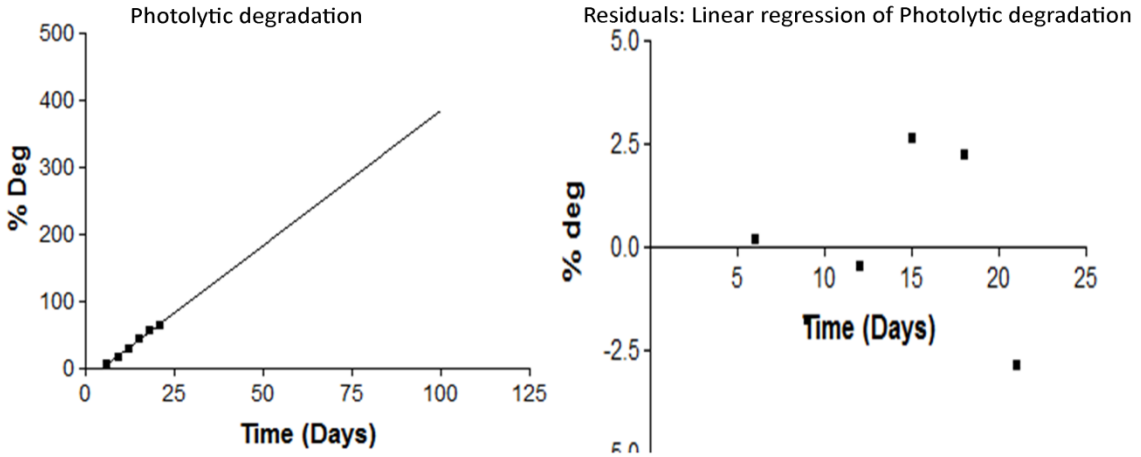

Figure 5.25: Zero order reaction kinetic and residual plot for photolytic degradation

5.6 SECTION-C

IMPURITY PROFILING AND DEGRADATION STUDY OF CICLOPIROX OLAMINE

5.6.1 EXPERIMENTAL

5.6.1.1 Chemicals and Reagents

The chemicals and reagents used in present section were same as described in section 3.4.1.1.

5.6.1.2 Equipments and Chromatographic Conditions

The equipments utilised in this section were same as described in section 3.4.1.2 and chromatographic conditions were same as described in section 5.4.1.2.

For LC–MS/MS analysis Ciclopirox Olamine (CIO) degradation samples were subjected to similar chromatographic conditions as mentioned in section 5.4.1.2. The m/z values obtained in positive ESI mode were compared to the molecular weights (MW) of the known degradation products (DPs) and to the inherent/process related impurities and/or DPs reported in drug monograph (European Pharmacopoeia (EP) (30)) or literature. The fragmentation patterns were also investigated. On the basis of MW and the fragmentation pattern, the presence of known process related or inherent impurities and/or DPs were confirmed and also structures of unknowns DPs were proposed and the fragmentation pathways were outlined.

5.6.1.3 Preparation of Stock, Sample and Buffer solutions

Stock, sample and buffer solutions were prepared in same way with similar dilutions as described in section 5.4.1.3.

5.6.2 RESULTS AND DISCUSSION

Three process related impurities of CIO (CIO IM-A, CIO IM-B and CIO IM-C) were specified in EU (30). The structures of reported process related impurities and related substances of CIO are provided in figure 5.26.

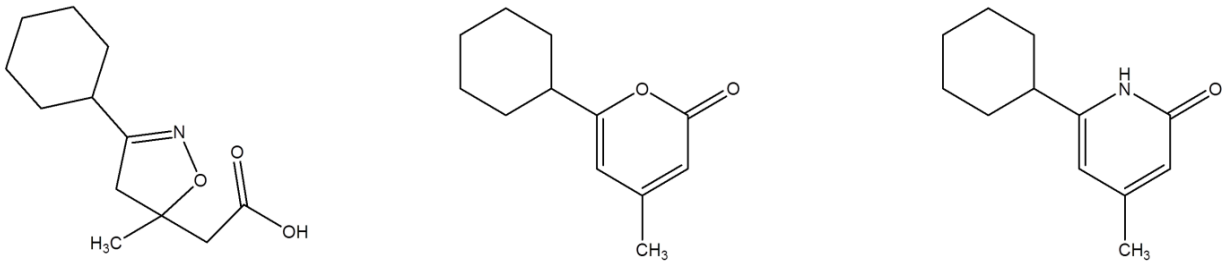

CIO IM-A

2-(3-cyclohexyl-4,5-dihydro-5-methylisoxazol-5-yl) acetic acid

Formula: $C_{12}H_{19}NO_3$

Mol Wt.: 225.28

CIO IM-B

2-6-cyclohexyl-4-methyl-2H-pyran-2-one

Formula: $C_{12}H_{16}O_3$

Mol Wt.: 192.25

CIO IM-C

6-cyclohexyl-4-methylpyridin-2(1H)-one

Formula: $C_{12}H_{16}O_3$

Mol Wt.: 191.27

Figure 5.26: Molecular structure of CIO related compounds

5.6.2.1 LC-PDA Study

Four DPs were observed by LC-PDA when CIO was subjected to stress degradation (described in section 5.4.2.5 and in figure 5.1.5). A process related impurities (CIO IM-C) was observed at Rt of 9.1 and is shown in figure 5.27. This processes related impurity was also formed during stress degradation and was identified as CIO IM-C after LC-MS/MS study with MW 191. Beside this, three other DPs were observed in LC-PDA and are summarized in table 5.20 in section 5.4.2.5.

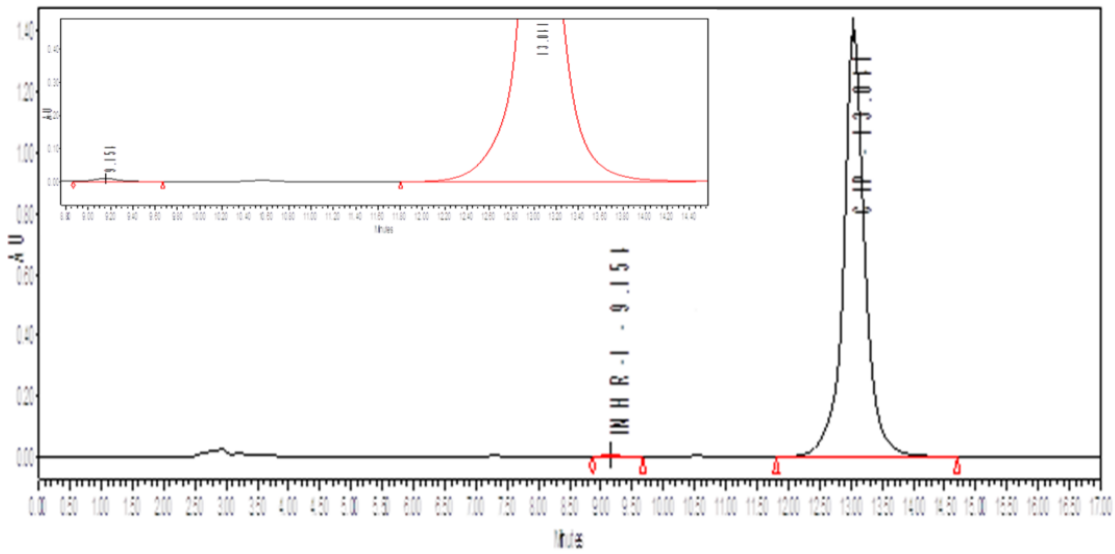

Figure 5.27: Chromatogram showing process related impurity

5.6.2.2 LC-MS/MS study and characterization of DPs

Four DPs were observed in LC-PDA and one additional DP i. e. DP-5 was observed in LC-MS/MS, which was observed as shouldered peak in LC-PDA under photolytic degradation.

MS/MS of CIO-M

The positive ion ESI-MS of CIO-M shows abundant [M+H]+ ion at m/z 222. The ESI-MS/MS spectrum (figure 5.28) of [M+H]+ ion of CIO-M showed most abundant product ions at m/z 123 corresponds to protonated prop-1-enyl-cyclohexane. The spectrum also include abundant product ions at m/z 192 due to the loss of CH_3OH from CIO-M, which further fragment to give product ions at m/z 163 due to the loss of CH_3OH+NO respectively. In addition, the spectrum also showed low abundant product ions at m/z 208 due to loss of CH_2 group which confirm the presence of the N-hydroxy group in the molecule. The proposed fragmentation pathway of CIO-M is shown in figure 5.30.

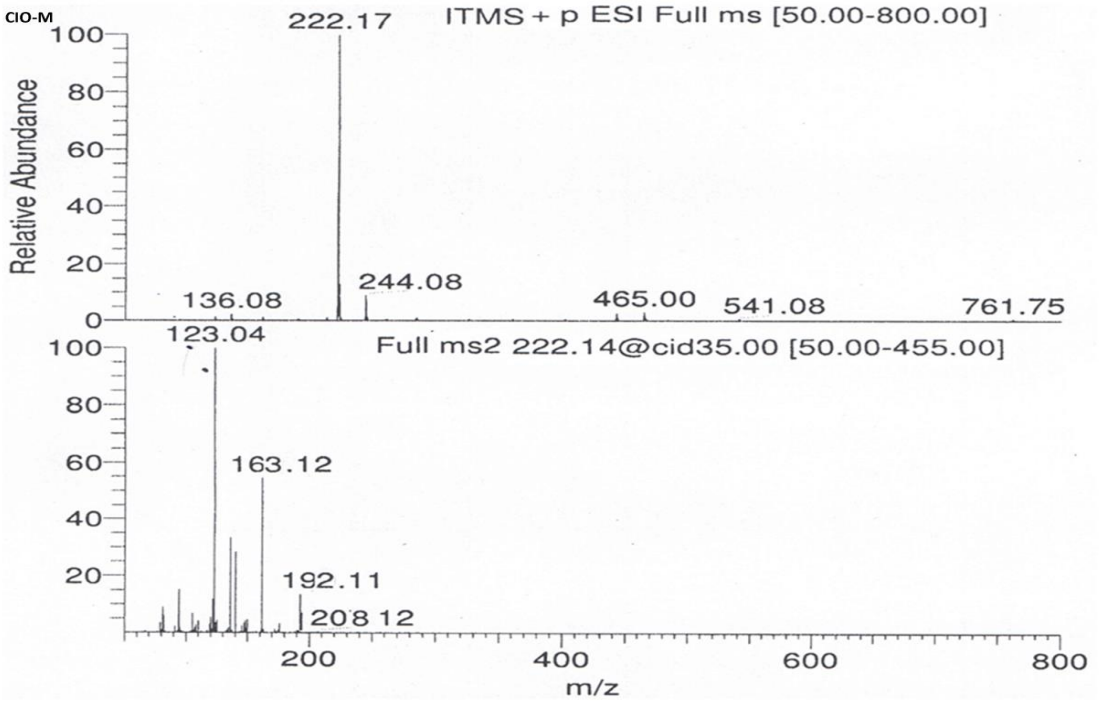

Figure 5.28: ESI-MS/MS spectra of CIO-M

DP-1 and DP-2 (m/z 236)

The positive ion ESI-MS of DP-1 and DP-2 showed abundant [M+H]+ ion at m/z 236. The ESI-MS/MS spectrum (figure 5.29) of [M+H]+ ion of DP-1 and DP-2 showed most abundant product ions at m/z 137 corresponds to but-1-enyl-cyclohexane.The spectrum also include abundant product ions at m/z 163, 150, and 124. The spectrum also showed low abundant product ions at m/z 222 and 110. m/z 222 corresponds to [M+H]+ of CIO-M formed by loss of CH_2 group from DP-1. The proposed fragmentation pathway of DP-1 and DP-2 are shown in figure 5.30.

Difference of DP-1 and DP-2

DP-1 and DP-2 could be isomeric in nature, as both have same MW. It was observed that DP-1 and DP-2 showed a few differences in their fragmentation pattern of [M+H]+ ions, however there were some common product ions. The MS/MS of DP-2 showed low abundant product ions at m/z 204 which was absent in the case of DP-1. The ion at m/z 222 and 163 were present in DP-1, while it was absent in case of DP-2. Abundant product ion with m/z 150, 137, and 123 are present in both DP-1 and DP-2.

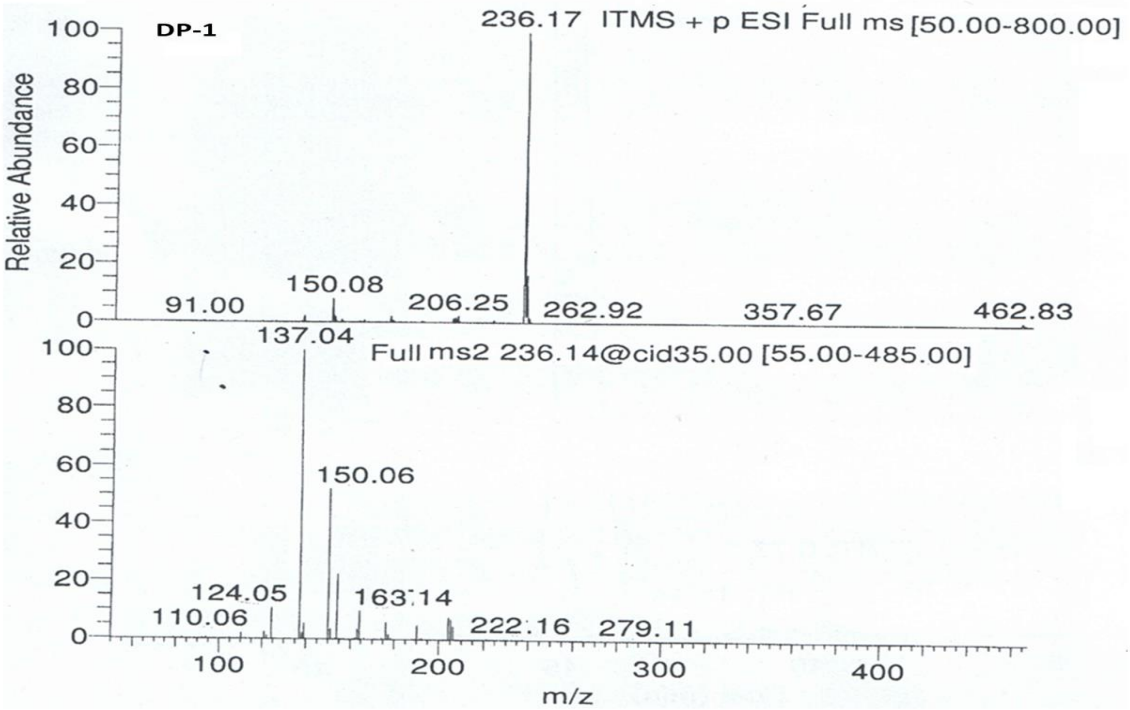

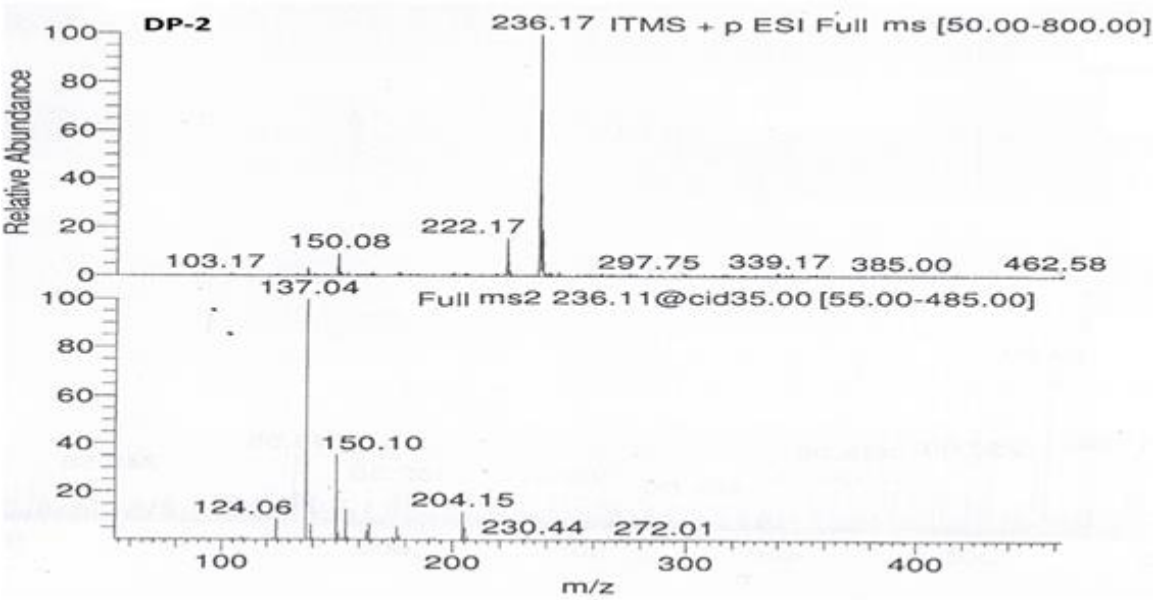

Figure 5.29: ESI-MS/MS spectra of DP-1 and DP-2

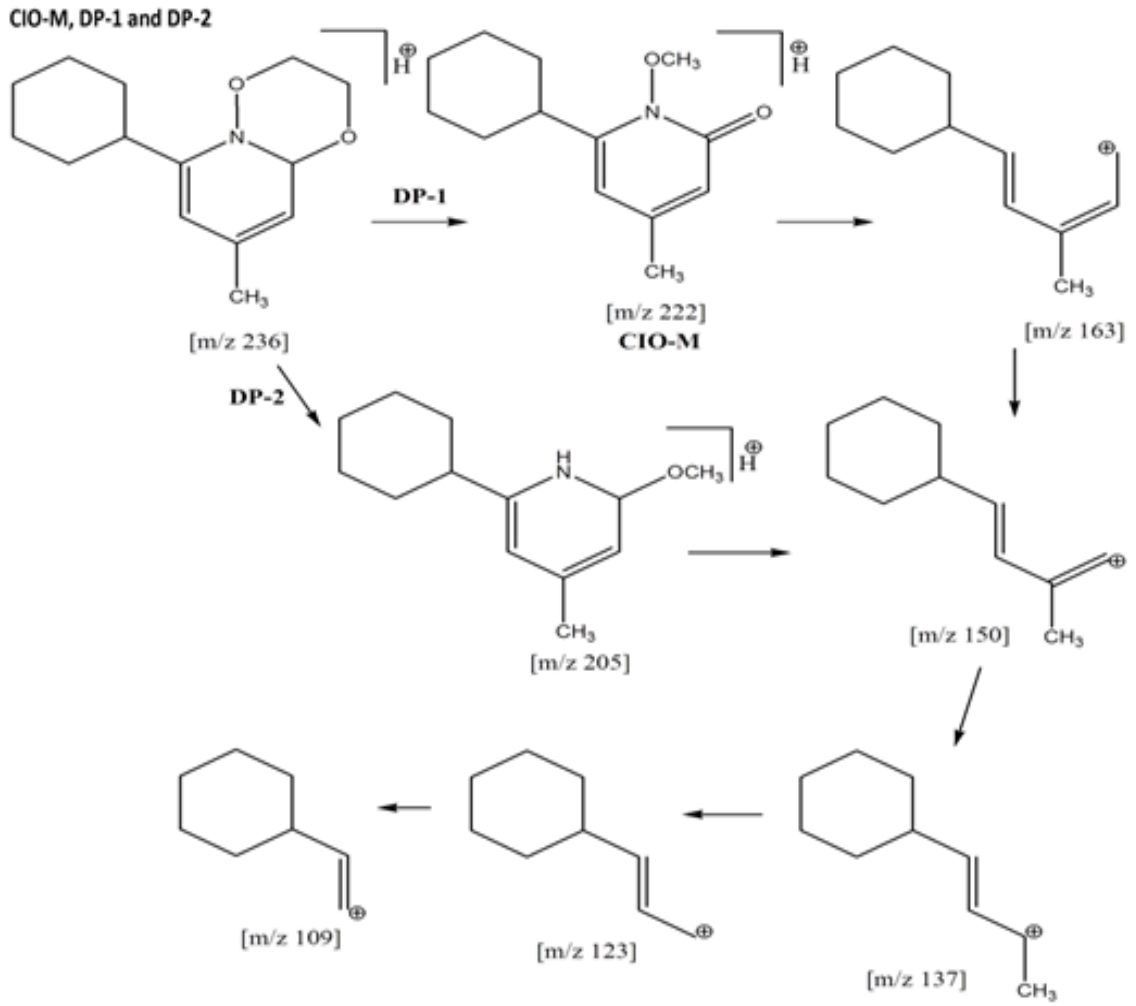

Figure 5.30: Proposed fragmentation pathway of CIO, DP-1 and DP-2.

DP-3 (m/z 192)

The ESI-MS/MS spectrum (figure 5.31) of the ion at m/z 192 (DP-3) showed the most abundant product ion at m/z 178, which is DP-5 formed by loss of oxygen. The ion m/z 149 is formed by the loss of $–CH_2NH$ group (29 Da) indicating the presence of amino group. The spectrum also include abundant product ions at m/z 109 due to the loss of C_3H_4, which further form product ion at 97 due to loss of one C. The MW of the parent and product ions confirms the proposed structure for DP-3, which is one of the process related impurity of CIO IM-C.

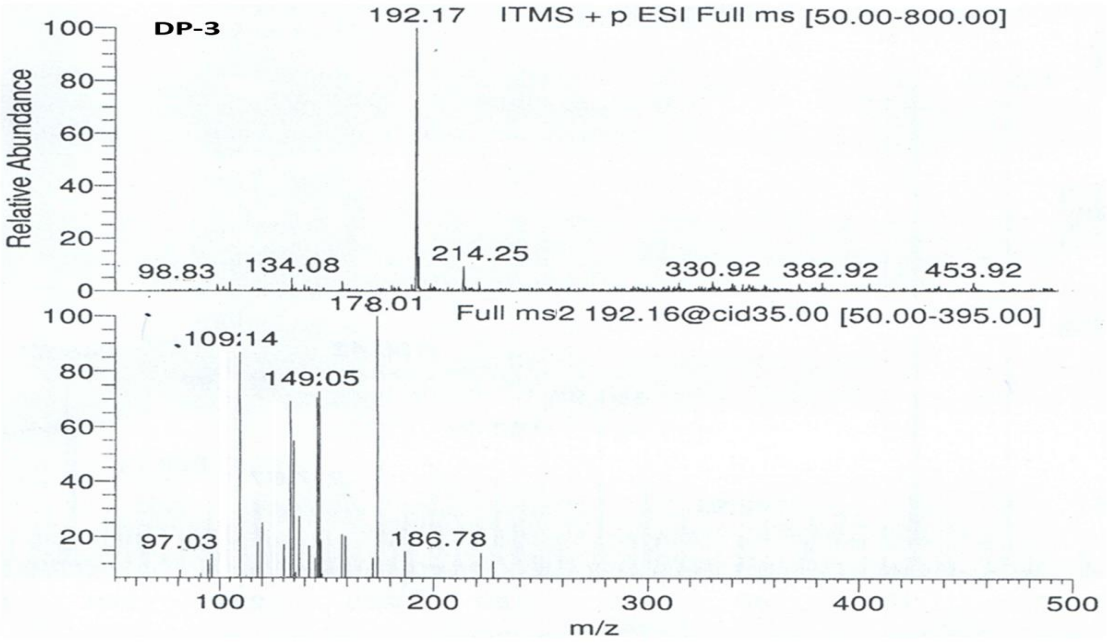

Figure 5.31: ESI-MS/MS spectra of DP-3

DP-4 (m/z 116)

The ESI-MS (figure 5.32) spectrum of the ion m/z 116 corresponding to the [M+H]+ of DP-4, that did not show protonated ions.

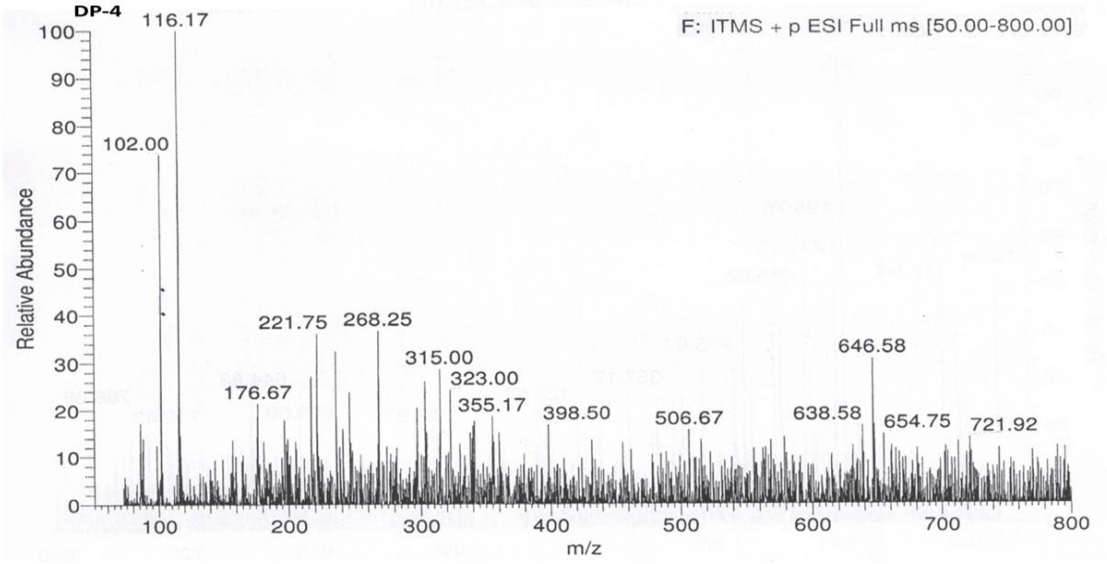

Figure 5.32: ESI-MS/MS spectra of DP-4

DP-5 (m/z 178)

The ESI-MS spectrum (figure 5.33) of the ion m/z 178 corresponding to the [M+H]+ of DP-5, that did not show protonated ions. The product ion with m/z 178 was formed from DP-3 by loss of oxygen. The proposed fragmentation pathway of DP-5 is shown in figure 5.34 that was formed from DP-3.

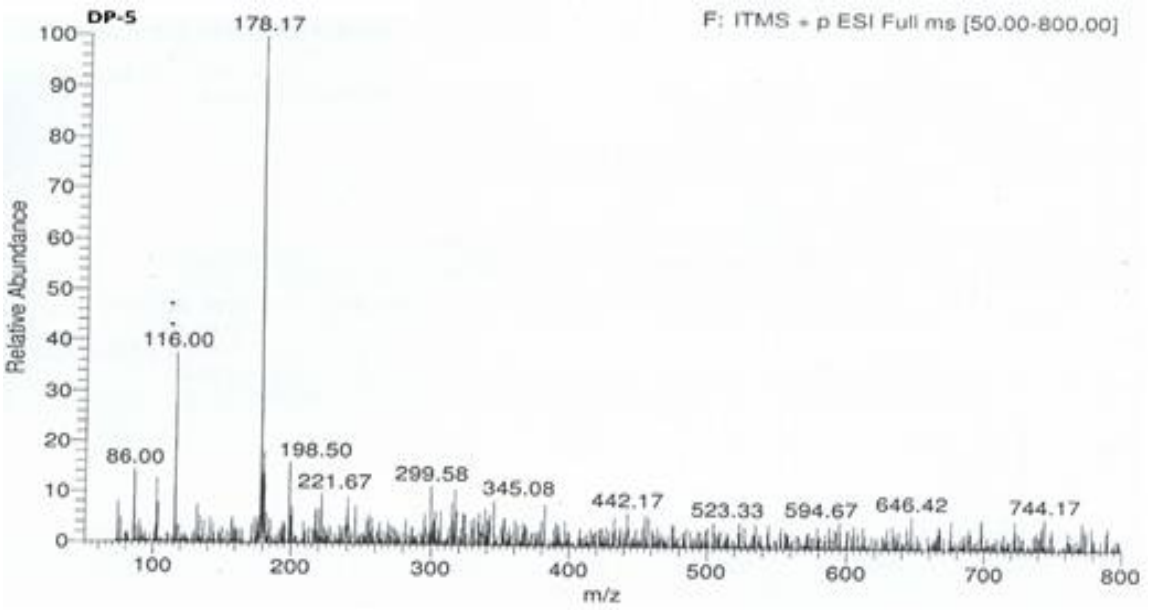

Figure 5.33: ESI-MS/MS spectra of DP-5

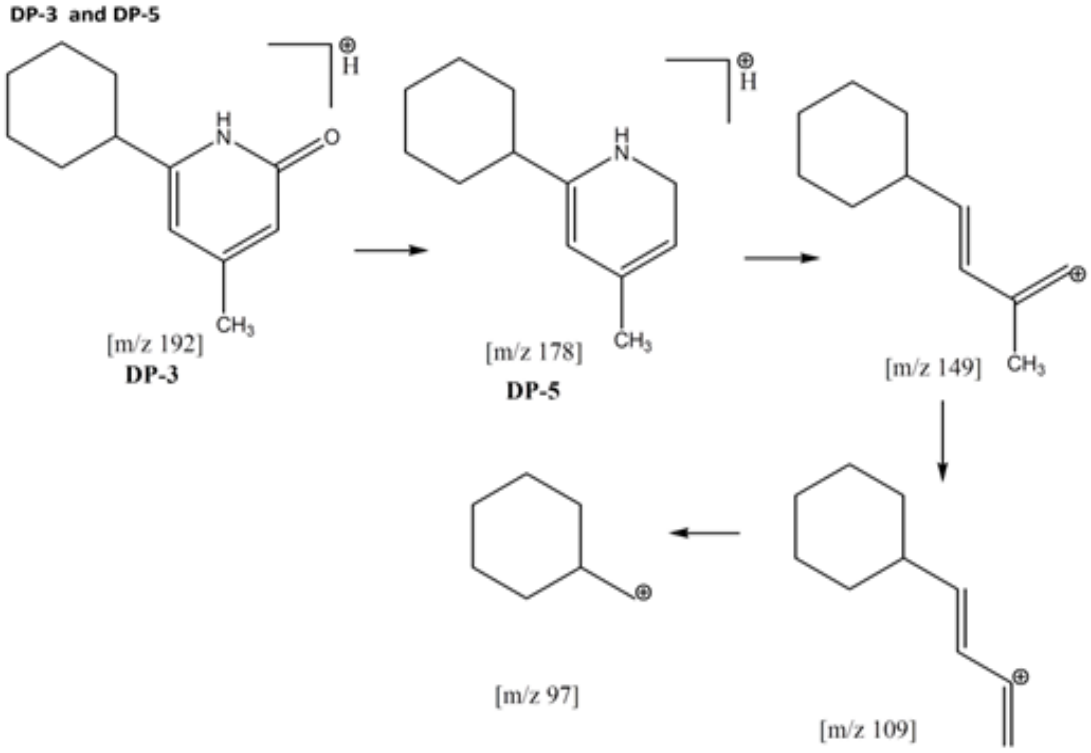

Figure 5.34: Proposed fragmentation pathway of DP-3 and DP-5

A schematic representation of CIO degradation showing formation of all DPs is shown in figure 5.35. Chemical structure of CIO and related compounds along with their origin, degradation route, Rt and observed m/z values for major fragments are shown in table 5.24. The structures and fragmentation pathways for CIO-M and DPs were proposed based on m/z values and fragmentation pattern.

It is clear from the table that CIO may contain 5 impurities which may be inherent (or process related) or degradation related. Out of 5 impurities identified, four impurities are not reported in literature.

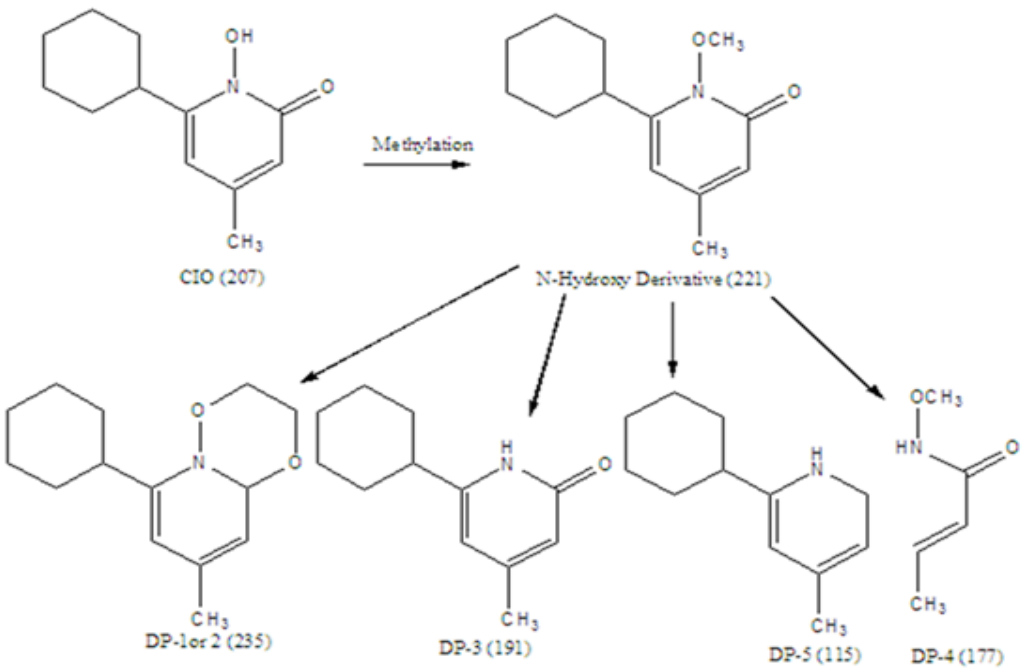

Figure 5.35: A schematic representation of CIO degradation

Table 5.24: Chemical structures of CIO and related compounds, their origin, degradation route, Rt and observed m/z values for major fragments

Analyte	Structure	Molecular formula molecular weight Fragments (m/z)	Origin	Degradation route	Rt (LC-PDA)
Ciclopirox (N-methoxy derivative)	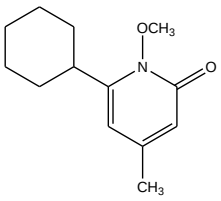	$C_{13}H_{19}NO_2$ 221.14 (208.12, 192.11, 163.12, 123.04)	API	--	12.7
IM-A	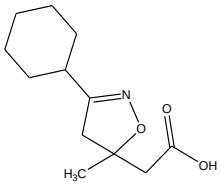	$C_{12}H_{17}NO_3$ 225.14	Process related	--	--

IM-B	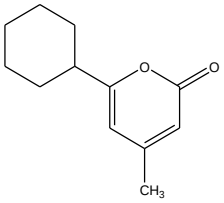	$C_{12}H_{16}O_2$ 192.12 (186.78, 178.01, 149.05, 109.14, 97.03)	Process related	--	--
IM-C and DP-3	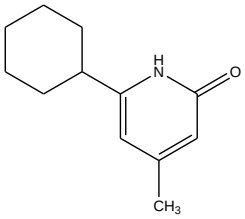	$C_{12}H_{17}NO$ 191.13	Process related Degradation product	Acid, base hydrolysis, oxidation and photolysis	8.9
DP-1	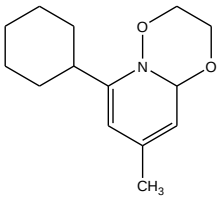	$C_{14}H_{21}NO_2$ 235.16 (222.16,163.14, 150.06,137.04, 124.05, 110.06)	Degradation product (unk)	Acid hydrolysis, Oxidation	7.1
DP-2	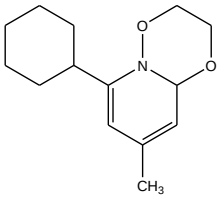	$C_{14}H_{21}NO_2$ 235.16 (230.44, 204.15, 150.10, 137.04, 124.06)	Degradation product (unk)	Acid, base Hydrolysis, Oxidation, Photolysis	7.5
DP-4	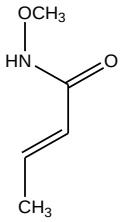	$C_5H_9NO_2$ 115.06	Degradation product (unk)	Acid and Base hydrolysis, oxidation	10.2
DP-5	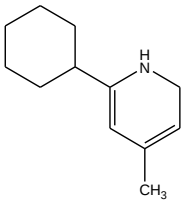	$C_{12}H_{19}N$ 177.29	Degradation product (unk)	Photolysis	Shouldered peak with Rt 10.7

5.7 CONCLUSION

To study the impurity profile and degradation behavior of CIO, the drug was subjected to ICH prescribed stress degradation conditions. Systematic profiling with utilization of QbD approach for optimization of HPLC separation method and MS detection lead to precise identification and monitoring of all major degradation products of CIO. Total five degradants were formed under stress conditions as identified by LC-MS/MS study. Stress degradation study revealed that CIO is most susceptible to photochemical degradation. It also undergoes significant degradation under acid, base hydrolysis and oxidation. The developed stability indicating assay method was successfully applied for estimation of CIO in topical formulations. No interference was observed from excipient present in solution. The developed method has been found to be accurate, selective, sensitive, and precise, and is applicable for estimation of possible degradants which may be present at trace level in bulk drugs and formulations. Besides, the method was validated based on ICH Q2(R1) guideline and total error approach. The degradation products formed in different stress conditions were characterized and possible structures of degradants were proposed through mass fragmentation studies. The molecular masses were established by recording LC-MS/MS scans in ESI mode and fragmentation pathways were outlined. The major degradation product DP-3 was identified as process related impurity (CIO IM-C) and was formed in almost all stress condition. Four other unreported degradation products of CIO were identified and characterized. It is hoped that characterization of the unknown degradation products of the CIO will be helpful to pharmaceutical industries in setting up their limits.

5.8 REFERENCES

1. Dittmar W, Lohaus G. HOE 296, a new antimycotic compound with a broad antimicrobial spectrum. Laboratory results. Arzneimittel-Forschung. 1973;23(5):670.

2. Dittmar W, Grau W, Raether W, Schrinner E, Wagner W. Microbiological laboratory studies with ciclopiroxolamine. Arzneimittel-Forschung. 1980;31(8A):1317-22.

3. Gasparini G, Contini D, Torti A, Guidarelli C, Lasagni A, Caputo R. The Effect of Ciclopirox Olamine Investigated by Means of the Freeze-Fracture Technique: Untersuchung der Wirkung von Ciclopiroxolamin mit der Freeze-Fracture-Technik. Mycoses. 1986;29(11):539-44.

4. Iwata K, Yamaguchi H. Studies on the mechanism of antifungal action of ciclopiroxolamine/Inhibition of transmembrane transport of amino acid, K+ and phosphate in Candida albicans cells. Arzneimittel-Forschung. 1980;31(8A):1323-7.

5. Clement PM, Hanauske Abel HM, Wolff EC, Kleinman HK, Park MH. The antifungal drug ciclopirox inhibits deoxyhypusine and proline hydroxylation, endothelial cell growth and angiogenesis in vitro. International Journal of Cancer. 2002;100(4):491-8.

6. Sakurai K, Sakaguchi T, Yamaguchi H, Iwata K. Mode of Action of 6-Cyclohexyl-l-hydroxy-4-methyl-2 (1H)-pyridone Ethanolamine Salt (HOE 296). Chemotherapy. 1978;24(2):68-76.

7. Eberhard Y, McDermott SP, Wang X, Gronda M, Venugopal A, Wood TE, et al. Chelation of intracellular iron with the antifungal agent ciclopirox olamine induces cell death in leukemia and myeloma cells. Blood. 2009;114(14):3064-73.

8. Lohaus G, Dittmar W. Process for the preparation of 1-hydroxy-pyridones. Google Patents, US3972888A; 1976.

9. Niewerth M, Kunze D, Seibold M, Schaller M, Korting HC, Hube B. Ciclopirox olamine treatment affects the expression pattern of Candida albicans genes encoding virulence factors, iron metabolism proteins, and drug resistance factors. Antimicrobial Agents and Chemotherapy. 2003;47(6):1805-17.

10. Sigle HC, Thewes S, Niewerth M, Korting HC, Schäfer Korting M, Hube B. Oxygen accessibility and iron levels are critical factors for the antifungal action of ciclopirox against Candida albicans. Journal of Antimicrobial Chemotherapy. 2005;55(5):663-73.

11. Subissi A, Monti D, Togni G, Mailland F. Ciclopirox. Drugs. 2010;70(16):2133-52.

12. XXIV USP. United States Pharmacopoeial Convention. Inc: Rockville, MD. 2006.

13. Belliardo F, Bertolino A, Brandolo G, Lucarelli C. Micro-liquid chromatography method for the determination of ciclopiroxolamine after pre-column derivatization in topical formulations. Journal of Chromatography A. 1991;553:41-5.

14. Lehr KH, Damm P. Quantification of ciclopirox by high-performance liquid chromatography after pre-column derivatization: An example of efficient clean-up using silica-bonded cyano phases. Journal of Chromatography B: Biomedical Sciences and Applications. 1985;339:451-6.

15. Coppi G, Silingardi S. HPLC method for pharmacokinetic studies on ciclopirox olamine in rabbits after intravenous and intravaginal administrations. Farmaco 1992;47(5):779-86.

16. Rockville M, editor United States Pharmacopeia 28-NF 23. United States Pharmacopeial Convention, INC; 2005.

17. Qadripur S, Horn G, Höhler T. On the local efficacy of ciclopiroxolamine in onychomycoses. Arzneimittel-Forschung. 1980;31(8A):1369-72.

18. Escarrone ALV, Bittencourt CF, Laporta LV, dos Santos MR, Primel EG, Caldas SS. LC–UV method with pre-column derivatization for the determination of ciclopirox olamine in raw material and topical solution. Chromatographia. 2008;67(11-12):967-71.

19. Samtsov A. Batrafen in the treatment of fungal diseases of the skin and nails. Voenno-medit͡sinskiĭ zhurnal. 2002;323(8):39.

20. Felix FS, do Lago CL, Angnes L. Determination of ciclopirox olamine in pharmaceutical products by capillary electrophoresis with capacitively coupled contactless conductivity detection. Electrophoresis. 2011;32(8):900-5.

21. Ibrahim F, El-Enany N. Polarographic determination of ciclopirox olamine in pure substance and in different pharmaceutical preparations. Il farmaco. 2003;58(12):1313-8.

22. Ibrahim F, El-Enany N. Anodic polarographic determination of ciclopirox olamine in pure and certain pharmaceutical preparations. Journal of Pharmaceutical and Biomedical Analysis. 2003;32(2):353-9.

23. Satani BH, Patel JV, Gami RB, Patel CN. Development and validation of a stability-indicating RP-HPLC method for estimation of Ciclopirox olamine in bulk drug and cream formulation. Journal of Pharmacy Research. 2013;6(1):102.

24. Gagliardi L, Multari G, Cavazzutti G, De Orsi D, Tonelli D. HPLC determination of ciclopirox, octopirox, and pyrithiones in pharmaceuticals and antidandruff preparations. Journal of Liquid Chromatography and Related Technologies. 1998;21(15):2365-73.

25. Li J, Jiang Y, Sun T, Ren S. Fast and simple method for assay of ciclopirox olamine by micellar electrokinetic capillary chromatography. Journal of Pharmaceutical and Biomedical Analysis. 2008;47(4):929-33.

26. Kim JH, Lee CH, Choi HK. A method to measure the amount of drug penetrated across the nail plate. Pharmaceutical Research. 2001;18(10):1468-71.

27. Ishikawa K, Lu DJ. What is total quality control?: the Japanese way: Prentice-Hall Englewood Cliffs, NJ; 1985.

28. Guideline. ICH Q2(R1) Validation of Analytical Procedures: methodology. European Agency for the Evaluation of Medicinal Products, International Commission on Harmonisation, London (CPMP/ICH/281/95). 1996.

29. Guideline IEC 17025: General Requirements for the Competence of Calibration and Testing Laboratories International Organization for Standardization. Geneva. 1999.

30. Pharmacopoeia. European Pharmacopoeia: Supplement: Council of Europe; 1998.